

Comprehensive application of a coupled-channel complex scaling method to the $\bar{K}N\text{-}\pi Y$ system

A. Doté^{a,b}, T. Inoue^c, T. Myo^d

^a*KEK Theory Center, Institute of Particle and Nuclear Studies (IPNS), High Energy Accelerator Research Organization (KEK), 1-1 Oho, Tsukuba, Ibaraki, 305-0801, Japan*

^b*J-PARC Branch, KEK Theory Center, IPNS, KEK, 203-1, Shirakata, Tokai, Ibaraki, 319-1106, Japan*

^c*Nihon University, College of Bioresource Sciences, Fujisawa 252-0880, Japan*

^d*Osaka Institute of Technology, Osaka, Osaka 535-8585, Japan*

Abstract

We have investigated $\bar{K}N\text{-}\pi Y$ system with a coupled-channel complex scaling method (ccCSM). By an advanced use of the ccCSM, scattering states as well as resonant states in the system have been treated in the same framework. Respecting the $\bar{K}N$ scattering length obtained by the Martin's analysis, we have constructed a meson-baryon potential matrix based on a chiral SU(3) theory, with a local Gaussian form in r -space. To test the property of the constructed potential, we have studied the scattering amplitude for isospin $I = 0$ and $I = 1$ channels and a resonant state in the $I = 0$ channel, in the ccCSM with both non- and semi-relativistic kinematics. The resonant pole corresponding to $\Lambda(1405)$ is found around (1419, -20) MeV ((1419, -13) MeV) on complex-energy plane with the non-relativistic (semi-relativistic) kinematics. Mean distance between meson and baryon in the resonant state is about $1.3 - i0.3$ ($1.2 - i0.5$) fm, which means that the state is considered as a Gamow state. We have observed a signature of another pole around ($\sim 1360, -40 \sim -90$) MeV, although it is unstable against change of scaling angle θ . This may correspond to the lower pole of the double-pole of $\Lambda(1405)$ discussed in literature today.

Keywords: $\bar{K}N\text{-}\pi Y$ system, $\Lambda(1405)$, scattering amplitude, complex scaling method, chiral SU(3) theory

Email address: dote@post.kek.jp (A. Doté)

1. Introduction

\bar{K} -nuclear system has been a hot topic in nuclear and hadron physics for a long time. Due to strongly attractive $\bar{K}N$ interaction in isospin $I = 0$ channel, finite nuclear systems with anti-kaons are expected to have exotic properties such as deeply bound and quasi-stable states with high density [1, 2]. Such kaonic nuclei have been investigated with various many-body treatments [2, 3, 4]. In particular, to clarify the property of kaonic nuclei, great efforts have been devoted to investigate K^-pp ¹, a prototype of kaonic nuclei, in both of theoretical and experimental studies. From the theoretical studies, it have been claimed that K^-pp will not be so deeply bound and its decay width will be large, (total binding energy < 100 MeV and decay width > 50 MeV) [1, 5, 6, 7, 8], although there are quantitative discrepancies between calculations [9]. On the other hand, experimental results indicate deeper binding of K^-pp than theoretical predictions if the observed state is the bound K^-pp [10, 11], although there are some objections to the experimental result [12]. Thus, the consensus for K^-pp has not been achieved yet.

For study of kaonic nuclei, $\bar{K}N$ (involving πY) interaction is a basic input, and a resonant $\Lambda(1405)$ is an essential building block because it can be reasonably interpreted as a quasi-bound $I = 0$ state of $\bar{K}N$ with s -wave, rather than a three-quark state [13]. One approach to $\bar{K}N$ system is a study based on the chiral $SU(3)$ coupled-channel dynamics [14]. This approach (called the chiral unitary model by Oset and Ramos [15]) has been succeeded in studies of s -wave meson-baryon systems including $S = -1$ sector [16]. The double pole nature of $\Lambda(1405)$ pointed out within this model, is interesting [17, 18]. According to further studies along this model, experimental data seem to support the double-pole nature [19]. Recently, accurate data at the $\bar{K}N$ threshold are given by a precise measurement of $1s$ level shift of kaonic hydrogen atom [20], in addition to experimental data on $\bar{K}N$ subthreshold region [21]. Due to such precise data, the physical quantities near the $\bar{K}N$ threshold are strictly constrained and those uncertainties below the $\bar{K}N$ threshold are also expected to be decreased [22].

In such a current situation, we start a study of kaonic nuclei with a coupled-channel complex scaling method (ccCSM), keeping in mind the fol-

¹Actually, this system is a $\bar{K}NN$ - πYN coupled system with quantum numbers $J^\pi = 0^-$, $(T, T_z) = (1/2, 1/2)$. It is expressed symbolically as K^-pp .

lowing three points: 1. Simple and adequate treatment of resonant states in many-body system, 2. Explicit inclusion of all channels in a coupled-channel problem, and 3. Accessible to structure of kaonic nuclei. Looking back past studies on K^-pp , in variational studies [1, 7] it is treated as a bound state in $\bar{K}NN$ channel as a consequence of the elimination of πY channels. In Faddeev-AGS studies [5, 6] certainly a coupled-channel calculation is fully performed and resonant poles are searched. However, there a separable form is assumed to the $\bar{K}N$ - πY potential which is a key ingredient in the \bar{K} nuclear study, and a wave function is not obtained explicitly in this approach though it is important to investigate the nature of kaonic nuclei. Thus, each approach involves advantages and disadvantages. Since the ccCSM is expected to overcome above disadvantages, we employ this method to study the \bar{K} nuclear system.

The complex scaling method (CSM) has been applied to various nuclear physics, and it has been greatly succeeded in particular in the study of resonant states of unstable nuclei [23]. The CSM is a practical tool for the study of nuclear many-body systems. Indeed, a resonant nature in unstable ^8He is revealed with the CSM in Ref. [24] where a five-body system of $^4\text{He} + n + n + n + n$ is solved. The CSM is suitable for resonant states, because we can handle them in the same way as bound states. Though a resonant wave function is originally divergent at infinite distance, in the CSM it is transformed to a square-integrable function by a complex rotation for the coordinate and then it can be represented with *e.g.* a Gaussian base which is familiar for ones study bound states. In addition, by an advanced used of complex-rotated wave functions, the scattering amplitude can also be calculated with the Gaussian base [25]. Thus, all of bound, resonant and scattering states can be handled in a single framework of the CSM with Gaussian base.

Since it is our first attempt applying the ccCSM to \bar{K} -nuclear systems, in this article we investigate the s -wave two-body system of $\bar{K}N$ - πY coupled channels. We examine semi-relativistic kinematics as well as non-relativistic one to be careful of a pion which is a light-mass particle. First, we will check how the ccCSM works in the present system. Then, we will construct a meson-baryon potential for the $\bar{K}N$ - πY coupled system, based on a chiral SU(3) theory. We adopt a Gaussian form in the coordinate space to the potential shape, because of convenience for our further study of \bar{K} -nuclear system with Gaussian base. Our potential is constrained by the $\bar{K}N$ scattering lengths for both isospin states obtained by the Martin's analysis of old

$\bar{K}N$ scattering data [26]. Using the constructed potential, we will investigate the behavior of the scattering amplitude. In the $I = 0$ sector, the pole on the complex-energy plane also will be investigated in detail because there should be a resonance corresponding to the $\Lambda(1405)$.

The contents of the article are as follows: In the section 2, we will explain a meson-baryon potential used in our study and the formalism of ccCSM for the study of scattering state as well as resonant state in detail. In the section 3, the obtained results will be given. The scattering amplitudes will be shown for both isospin states. For the $I = 0$ channel, the structure of a resonant state will be investigated. In the last section, we will mention our summary and future plans including some discussions.

2. Formalism

2.1. Kinematics and interaction

We are considering a $\bar{K}N\text{-}\pi Y$ coupled system in s -wave, where Y indicates a hyperon which is Σ (Λ and Σ) for $I = 0$ ($I = 1$) case. We investigate such a two-body system in semi-relativistic kinematics as well as non-relativistic one, because a pion joins in our calculation and its mass is very small. The Hamiltonian for non-relativistic kinematics is

$$\hat{H} = \sum_{\alpha} \left(M_{\alpha} + m_{\alpha} + \frac{\hat{\mathbf{p}}_{\alpha}^2}{2\mu_{\alpha}} \right) |\alpha\rangle\langle\alpha| + \hat{V}_{MB}^{NR}, \quad (1)$$

and that for semi-relativistic kinematics is

$$\hat{H} = \sum_{\alpha} \left(\sqrt{M_{\alpha}^2 + \hat{\mathbf{p}}_{\alpha}^2} + \sqrt{m_{\alpha}^2 + \hat{\mathbf{p}}_{\alpha}^2} \right) |\alpha\rangle\langle\alpha| + \hat{V}_{MB}^{SR}. \quad (2)$$

Here M_{α} , m_{α} and μ_{α} are baryon, meson and a reduced mass in the channel α , respectively. $\hat{\mathbf{p}}_{\alpha}$ is the relative momentum between a meson and a baryon in the channel α .

The last term \hat{V}_{MB}^{NR} (\hat{V}_{MB}^{SR}) represents a meson-baryon potential for non-relativistic (semi-relativistic) kinematics. In Ref. [14], Kaiser, Siegel and Weise proposed a pseudo-potential for meson-baryon system with $S = -1$ derived from an effective chiral SU(3) Lagrangian, and used it in a Lippmann-Schwinger equation to obtain $\Lambda(1405)$. In this paper we follow this work and

adopt the lowest order of the pseudo-potential:

$$\hat{V}_{MB}^{SR} = \sum_{\alpha,\beta} -\frac{C_{\alpha\beta}^I}{f_\pi^2}(\omega_\alpha + \omega_\beta) \sqrt{\frac{M_\alpha M_\beta}{s \tilde{\omega}_\alpha \tilde{\omega}_\beta}} g_{\alpha\beta}^I(r) |\alpha\rangle\langle\beta|, \quad (3)$$

$$g_{\alpha\beta}^I(r) = (\sqrt{\pi} d_{\alpha\beta}^I)^{-3} \exp[-(r/d_{\alpha\beta}^I)^2], \quad (4)$$

where the spatial dependence is modified from the δ function in the original to a Gaussian function with a range parameter $d_{\alpha\beta}^I$. Hereafter, we denote this as “KSW potential”. Note that this potential is energy dependent because meson energy ω_α , baryon energy E_α and the reduced energy $\tilde{\omega}_\alpha = \omega_\alpha E_\alpha / (\omega_\alpha + E_\alpha)$ are given by function of CM energy \sqrt{s} as follows:

$$E_\alpha = \frac{(\sqrt{s})^2 - m_\alpha^2 + M_\alpha^2}{2\sqrt{s}} \quad \text{and} \quad \omega_\alpha = \frac{(\sqrt{s})^2 + m_\alpha^2 - M_\alpha^2}{2\sqrt{s}}. \quad (5)$$

Note also that structure of this potential is determined by the coefficients $\{C_{\alpha\beta}^I\}$ which are computed by Clebsch-Gordan coefficients of SU(3) and given as

$$C^{(I=0)} = \begin{pmatrix} \bar{K}N & \pi\Sigma \\ 3 & -\sqrt{3/2} \\ & 4 \end{pmatrix}, \quad C^{(I=1)} = \begin{pmatrix} \bar{K}N & \pi\Sigma & \pi\Lambda \\ 1 & -1 & -\sqrt{3/2} \\ & 2 & 0 \\ & & 0 \end{pmatrix}. \quad (6)$$

Strength of this potential depends on the pion decay constant f_π . It is noted that the range parameter $d_{\alpha\beta}^I$ can be a different value in each channel set (α, β) . For the range parameter of the transition potential, we assume that $d_{\alpha\beta}^I = (d_{\alpha\alpha}^I + d_{\beta\beta}^I)/2$ to reduce the number of parameters.

Since the flux factor $\sqrt{\frac{M_\alpha M_\beta}{s \tilde{\omega}_\alpha \tilde{\omega}_\beta}}$ in Eq. (3) is based on the relativistic kinematics, the KSW potential had better be used in the semi-relativistic framework in our calculation. When we adopt the non-relativistic kinematics, we make non-relativistic reduction to the flux factor in two prescriptions, denoted as “NRv1” and “NRv2”. In the first prescription, comparing the expression of the differential cross section in both kinematics, we replace the reduced energy in Eq. (3) with the reduced mass;

$$\text{NRv1 : } \hat{V}_{MB}^{NRv1} = \sum_{\alpha,\beta} -\frac{C_{\alpha\beta}^I}{f_\pi^2}(\omega_\alpha + \omega_\beta) \sqrt{\frac{M_\alpha M_\beta}{s \mu_\alpha \mu_\beta}} g_{\alpha\beta}^I(r) |\alpha\rangle\langle\beta|. \quad (7)$$

In the second prescription, by considering the small momentum limit, we replace the meson and baryon energies with the meson and baryon masses, respectively;

$$\text{NRv2 : } \hat{V}_{MB}^{NRv2} = \sum_{\alpha,\beta} -\frac{C_{\alpha\beta}^I}{f_\pi^2} (\omega_\alpha + \omega_\beta) \sqrt{\frac{1}{m_\alpha m_\beta}} g_{\alpha\beta}^I(r) |\alpha\rangle\langle\beta|. \quad (8)$$

In both non-relativistic approximations, we keep remaining the meson-energy part $(\omega_\alpha + \omega_\beta)$ as original, because this energy dependence is attributed to the chiral dynamics which we respect in our study. Of course, energies such as \sqrt{s} and ω_α themselves, are calculated by the non-relativistic formula.

2.2. Coupled-channel complex scaling method

As mentioned in the introduction, the s -wave $\bar{K}N$ - $\pi\Sigma$ system has a resonant state in $I = 0$ channel which corresponds to the $\Lambda(1405)$. Such a resonant state of a meson-baryon system can also be investigated with the complex scaling method (CSM), in the same way as resonant states of unstable nuclei. Here, we give a brief explanation of the coupled-channel complex scaling method (ccCSM). Details of the CSM and its successful application to unstable nuclear physics are summarized in Ref. [23]

In the CSM, a relative coordinate \mathbf{r} and a conjugate wave number \mathbf{k} in Hamiltonian \hat{H} and a wave function $|\Phi\rangle$ are complex-scaled as

$$U(\theta) : \mathbf{r} \rightarrow \mathbf{r}e^{i\theta}, \mathbf{k} \rightarrow \mathbf{k}e^{-i\theta}. \quad (9)$$

Then, transformed Hamiltonian and wave function are defined as $\hat{H}_\theta \equiv U(\theta)\hat{H}U^{-1}(\theta)$ and $|\Phi_\theta\rangle \equiv U(\theta)|\Phi\rangle$, respectively. We expand the wave function $\Phi(\mathbf{r})$ in partial waves as $\Phi(\mathbf{r}) = \sum_{lm} \phi_l(r)/r Y_{lm}(\Omega)$ as usual. In our definition, all radial wave functions are transformed by the complex scaling operator as

$$\phi_l^\theta(r) \equiv U(\theta)\phi_l(r) = e^{i\theta/2}\phi_l(re^{i\theta}), \quad (10)$$

taking into account the Jacobian in integration to calculate expectation value of operators. An expectation value of operator \hat{O} is calculated with bi-orthogonal set $\{\tilde{\Phi}_\theta\}$:

$$\langle\hat{O}\rangle_\theta \equiv \langle\tilde{\Phi}_\theta|\hat{O}|\Phi_\theta\rangle, \quad (11)$$

where $\tilde{\Phi}_\theta(r) = \Phi_\theta^*(r)$ in terms of radial part of wave function for bound and resonant states. The complex scaled wave function is generally normalized as $\langle \tilde{\Phi}_\theta | \Phi_\theta \rangle = 1$. With the definition of the bi-orthogonal state, the radial part of the complex scaled wave function is normalized as

$$\sum_l \int_0^\infty dr \{ \phi_l^\theta(r) \}^2 = 1 \quad (12)$$

for bound and resonant states [23].

It is known that energies of bound and resonant states are independent of the scaling angle θ while those of continuum states vary with θ as $\frac{k^2}{2m} e^{-2i\theta}$ in case of non-relativistic kinematics. (*ABC theorem* [23]) In addition, it is easily understood that a resonant wave function is transformed from a divergent function to a dumping function by the complex scaling $U(\theta)$ with adequate values of θ . In other words, the boundary condition for resonant states is modified to the same one for bound states. Therefore, we can obtain resonant states as follows: For various θ 's, complex eigenvalues are calculated by diagonalizing the complex-scaled Hamiltonian \hat{H}_θ with Gaussian base as done in usual studies of bound states. Among obtained eigenstates, the states with the eigenvalues independent of θ are recognized as resonant states. Since the continuum states appear along a line $\tan^{-1}(E_I/E_R) = -2\theta$ on the complex-energy plane, resonant states can be separated from the continuum states when we set the scaling angle θ appropriately. Similarly, resonant states can be found also in case of semi-relativistic kinematics, although complex eigenvalues of continuum states have different θ -dependence from non-relativistic case.

In the present study, the CSM is applied to a coupled-channel problem, because the $I = 0$ wave function contains the $\bar{K}N$ and $\pi\Sigma$ components. The spatial parts of these wave functions with s -wave, $\phi_{\bar{K}N}(r)$ and $\phi_{\pi\Sigma}(r)$, are expanded with Gaussian base $G_n^\alpha(r)$:

$$|\Phi_{\bar{K}N-\pi\Sigma}^{I=0,l=0}\rangle = \frac{1}{r} \phi_{\bar{K}N}^{l=0}(r) Y_{00}(\Omega) |\bar{K}N\rangle + \frac{1}{r} \phi_{\pi\Sigma}^{l=0}(r) Y_{00}(\Omega) |\pi\Sigma\rangle \quad (13)$$

$$\phi_\alpha^{l=0}(r) = \sum_j C_j^\alpha G_j(r) = \sum_j C_j^\alpha N_{l=0}(b_j) r \exp[-r^2/2b_j^2], \quad (14)$$

where coefficients $\{C_n^\alpha\}$ are complex parameters to be determined. As explained above, by diagonalizing the \hat{H}_θ with the basis $\{G_n^\alpha(r)|\alpha\rangle\}$ and investigating the θ dependence of eigenvalues, we can find resonant states. As

explained in Eq. (12), the radial part of the $I = 0$ wave function (Eq. (13)) is normalized as

$$\int_0^\infty dr \left[\left\{ \phi_{\bar{K}N,\theta}^{l=0}(r) \right\}^2 + \left\{ \phi_{\pi\Sigma,\theta}^{l=0}(r) \right\}^2 \right] = 1, \quad (15)$$

when it is complex-scaled.

Note that the self-consistency for the complex energy is needed to be considered, since the meson-baryon potentials (Eqs. (3), (7) and (8)) have an energy dependence attributed to chiral dynamics. The eigen energy E_{calc} of Hamiltonian calculated with the ccCSM should coincide with the energy E_{int} inputted into the meson-baryon potential as $\hat{V}_{MB}(\sqrt{s} = E_{int})$. Here E_{calc} and E_{int} are complex values because they are the energies of resonant states, $E_R - i\Gamma/2$. (E_R and Γ are energy and decay width, respectively) At the n -th iteration, we set a value of $E_{int}^{(n)}$ as an input for the \hat{V}_{MB} and then obtain an eigen energy $E_{calc}^{(n)}$ of resonant state with ccCSM. We use the $E_{calc}^{(n)}$ as an input $E_{int}^{(n+1)}$ for the next term. Such iterations are repeated until the self-consistent condition is satisfied; $E_{calc}^{(n)} = E_{int}^{(n)}$. In case of the present system, the self-consistency is achieved in five-times iterations [27]. ($n \leq 5$)

2.3. Scattering amplitude calculated with ccCSM — “CS-WF” method—

We are interested in the scattering state as well as the resonant state which can be investigated with the usual CSM as explained in the previous section. In this article, we solve a scattering problem also with a square-integrable base such as Gaussian base with the help of the CSM, following a method called “CS-WF” which was developed by Kruppa, Suzuki and Kato [25]. Here, the detailed formalism of CS-WF is shown for a multi-channel case such as the $\bar{K}N$ - πY system.

We assume a system involving n channels in which the channel c_0 is the incident channel with the energy E . In a non-relativistic case, the radial Schrödinger equation for such a multi-channel system is

$$(E - H_c^l) \Phi_{l,c}^{(c_0)}(r) = \sum_{c'=1}^n V_{cc'} \Phi_{l,c'}^{(c_0)}(r), \quad (16)$$

$$H_c^l = -\frac{\hbar^2}{2\mu_c} \frac{d^2}{dr^2} + \frac{\hbar^2}{2\mu_c} \frac{l(l+1)}{r^2} + V_{D,c}(r) + M_{T,c}, \quad (17)$$

where μ_c and $M_{T,c}$ are the reduced mass and the total mass in the channel c , respectively. $V_{D,c}(r)$ is a direct potential for the channel c and $V_{cc'}$ is

a transition potential between channels c and c' . We assign closed (open) channels for the incident energy E to channel numbers $c = 1 \sim n_B$ ($c = n_B + 1 \sim n$). The wave function of the channel c can be written as

$$\Phi_{l,c}^{(c_0)}(r) = \begin{cases} \psi_{l,c}^{(c_0),B}(r) & (c = 1, \dots, n_B) \\ \hat{j}_l(k_{c_0}r) \delta_{c,c_0} + \psi_{l,c}^{(c_0),sc}(r) & (c = n_B + 1, \dots, n) \end{cases} \quad (18)$$

The incident wave number k_{c_0} satisfies $\frac{\hbar^2}{2\mu_{c_0}}k_{c_0}^2 + M_{T,c_0} = E$.

Inserting this equation into Eq. (16) and applying the complex scaling, then we obtain the coupled equations as follows:

$$\begin{aligned} & (E - H_c^{l,\theta}) \begin{Bmatrix} \psi_{l,c}^{(c_0),B,\theta}(r) \\ \psi_{l,c}^{(c_0),sc,\theta}(r) \end{Bmatrix} \\ & - \sum_{c'=1}^{n_B} V_{cc'}(re^{i\theta}) \psi_{l,c'}^{(c_0),B,\theta}(r) - \sum_{c'=n_B+1}^n V_{cc'}(re^{i\theta}) \psi_{l,c'}^{(c_0),sc,\theta}(r) \\ & = e^{i\theta/2} V_{cc_0}(re^{i\theta}) \hat{j}_l(kre^{i\theta}) \begin{cases} (c = 1, \dots, n_B) \\ (c = n_B + 1, \dots, n) \end{cases}, \end{aligned} \quad (19)$$

where $\psi_{l,c}^{(c_0),B,\theta}(r)$ ($\psi_{l,c}^{(c_0),sc,\theta}(r)$) means the $\psi_{l,c}^{(c_0),B}(r)$ ($\psi_{l,c}^{(c_0),sc}(r)$) complex-scaled as following Eq. (10). The complex-scaled Hamiltonian for the channel c is

$$H_c^{l,\theta} = -e^{-2i\theta} \frac{\hbar^2}{2\mu_c} \frac{d^2}{dr^2} + e^{-2i\theta} \frac{\hbar^2}{2\mu_c} \frac{l(l+1)}{r^2} + V_{D,c}(re^{i\theta}) + M_{T,c}. \quad (20)$$

The wave functions for the closed channels, $\{\psi_{l,c}^{(c_0),B}(r)\}$, are square-integrable since the threshold energy of these channels is above the incident energy E . The complex-scaled ones are also square-integrable. As for the open channels whose threshold energies are below the E , the scattered part of wave functions, $\{\psi_{l,c}^{(c_0),sc}(r)\}$, are not square-integrable, since they behave in the asymptotic region as

$$\psi_{l,c}^{(c_0),sc}(r) \rightarrow k_c f_{l,cc_0}(k_c) \hat{h}_l^{(+)}(k_c r) \propto \exp\{i(k_c r - l\pi/2)\} \quad \text{at } r \rightarrow \infty, \quad (21)$$

where $\hat{h}_l^{\pm}(kr)$ is the Riccati-Hankel function. But, they are transformed to be square-integrable functions due to the complex scaling. The asymptotic behavior of the complex-scaled scattered part of wave function is

$$\psi_{l,c}^{(c_0),sc,\theta}(r) \propto i^{-l} \exp\{ik_c r \cos \theta - k_c r \sin \theta\} \quad \text{at } r \rightarrow \infty. \quad (22)$$

It is easy to understand that the $\psi_{l,c}^{(c_0),sc,\theta}$ becomes a square-integrable function for $0 < \theta < \pi$. Thus, since both the complex-scaled wave functions $\{\psi_{l,c}^{(c_0),B,\theta}(r)\}$ and $\{\psi_{l,c}^{(c_0),sc,\theta}(r)\}$ are square-integrable, they can be expanded with Gaussian base $\{G_i(r)\}$ as

$$\begin{Bmatrix} \psi_{l,c}^{(c_0),B,\theta}(r) \\ \psi_{l,c}^{(c_0),sc,\theta}(r) \end{Bmatrix} \equiv \psi_{l,c}^{(c_0),\theta}(r) = \sum_{j=1}^N t_{c,j}^{(c_0)}(\theta) G_j(r). \quad (23)$$

In the present study, we use a common set of normalized Gaussians for all channels:

$$G_i(r) = N_l(b_i) r^{l+1} \exp\left[-\frac{r^2}{2b_i^2}\right], \quad N_l(b_i) = b_i^{-(2l+3)/2} \left\{ \frac{2^{l+2}}{(2l+1)!!\sqrt{\pi}} \right\}. \quad (24)$$

Inserting the Eq. (23) into the coupled equations (19), linear equations for the unknown variables $\{t_{c,i}^{(c_0)}(\theta)\}$ are obtained:

$$\sum_j \left[\left(E O_{ij} - H_{c,ij}^{l,\theta} \right) t_{c,j}^{(c_0)}(\theta) - \sum_{c'=1}^n V_{cc',ij}^\theta t_{c',j}^{(c_0)}(\theta) \right] = b_{cc_0,i}^\theta, \quad (25)$$

where each matrix element indicates $O_{ij} = \langle G_i | G_j \rangle$, $H_{c,ij}^{l,\theta} = \langle G_i | H_c^{l,\theta} | G_j \rangle$, $V_{cc',ij}^\theta = \langle G_i | V_{cc'}(r e^{i\theta}) | G_j \rangle$ and

$$b_{cc_0,i}^\theta = e^{i\theta/2} \int_0^\infty dr G_i(r) V_{cc_0}(r e^{i\theta}) \hat{j}_l(k r e^{i\theta}). \quad (26)$$

We explain how to calculate scattering amplitudes in the remaining part of this section. With the scattering wave functions $\{\Phi_{l,c}^{(c_0)}(r)\}$, the scattering amplitude between the initial channel c_0 and the final channel c is expressed as

$$f_{l,cc_0}(k_c) = -\frac{\mu_c}{\hbar^2 k_c k_{c_0}} \sum_{c'=1}^n \int_0^\infty dr \hat{j}_l(k_c r) V_{cc'}(r) \Phi_{l,c'}^{(c_0)}(r). \quad (27)$$

It is obtained with the help of Green function, as a detailed explanation is given in Appendix A. By inserting Eq. (18) into the $\Phi_{l,c'}^{(c_0)}(r)$ of the above equation, the full scattering amplitude is decomposed to the Born term $f_{l,cc_0}^{Born}(k_c)$ attributed to the incoming wave $\hat{j}_l(k_{c_0} r)$ and the other part

$f_{l,cc_0}^{sc}(k_c)$ attributed to the scattered wave $\psi_{l,c}^{(c_0)}(r)$. The Born term can be obtained by the numerical integration. In the calculation of $f_{l,cc_0}^{sc}(k_c)$, the integration path can be modified from r -axis to $re^{i\theta}$ -line due to the Cauchy's theorem. Therefore, the $f_{l,cc_0}^{sc}(k_c)$ is equal to $f_{l,cc_0}^{sc,\theta}(k_c)$ that can be calculated with the complex-scaled wave functions $\{\psi_{l,c}^{(c_0),\theta}(r)\}$, as

$$f_{l,cc_0}^{sc,\theta}(k_c) = -\frac{\mu_c}{\hbar^2 k_c k_{c_0}} e^{i\theta/2} \sum_{c'=1}^n \int_0^\infty dr \hat{j}_l(k_c r e^{i\theta}) V_{cc'}(r e^{i\theta}) \psi_{l,c}^{(c_0),\theta}(r). \quad (28)$$

Thus, we can obtain the full scattering amplitudes as

$$f_{l,cc_0}(k_c) = f_{l,cc_0}^{Born}(k_c) + f_{l,cc_0}^{sc}(k_c) \quad (29)$$

$$f_{l,cc_0}^{Born}(k_c) = -\frac{\mu_c}{\hbar^2 k_c k_{c_0}} \int_0^\infty dr \hat{j}_l(k_c r) V_{cc_0}(r) \hat{j}_l(k_{c_0} r) \quad (30)$$

$$f_{l,cc_0}^{sc}(k_c) = f_{l,cc_0}^{sc,\theta}(k_c) \simeq -\frac{\mu_c}{\hbar^2 k_c k_{c_0}} \sum_{c'=1}^n \sum_{j=1}^N t_{c',j}(\theta) b_{c',c,i}^\theta. \quad (31)$$

The $f_{l,cc_0}^{sc,\theta}(k_c)$ can be obtained with the matrix elements $\{b_{c',c,i}^\theta\}$ by using the Eqs. (23) and (26).

We summarize the essential points of the CS-WF at the end of this section. The first point is that the incoming part $\hat{j}_l(k_{c_0} r)$ is separated from the scattered wave functions $\{\psi_{l,c}^{(c_0),sc}(r)\}$ as shown in Eq. (18) and that only the scattered parts $\{\psi_{l,c}^{(c_0)}(r)\}$ are complex-scaled. The complex scaling is used to make a non-square integrable function transformed to a square integrable one. If the full scattering wave function $\Phi_{l,c}^{(c_0)}(r)$ is complex-scaled, it does not become a square-integrable function because of Riccati-Bessel function $\hat{j}_l(k_{c_0} r)$ that contains both components of $\exp\{\pm i(kr - \frac{l\pi}{2})\}$ in the asymptotic region. The second point is that we calculate the scattering amplitude with the complex-scaled function $\psi_{l,c}^{(c_0),\theta}(r)$, instead of the $\psi_{l,c}^{(c_0)}(r)$ which is needed in usual calculation of the scattering amplitude. By the Cauchy's theorem, the amplitude can be obtained with the $\psi_{l,c}^{(c_0),\theta}(r)$ which is expressed with a square-integrable base. We note that the scattering amplitudes calculated in this way are independent of the scaling angle θ .

In case of the semi-relativistic kinematics, the scattering amplitudes are calculated in the same way as the non-relativistic kinematics as explained above, by replacing the matrix elements of kinetic energy term with those for the semi-relativistic kinematics. These matrix elements are given in Appendix B.

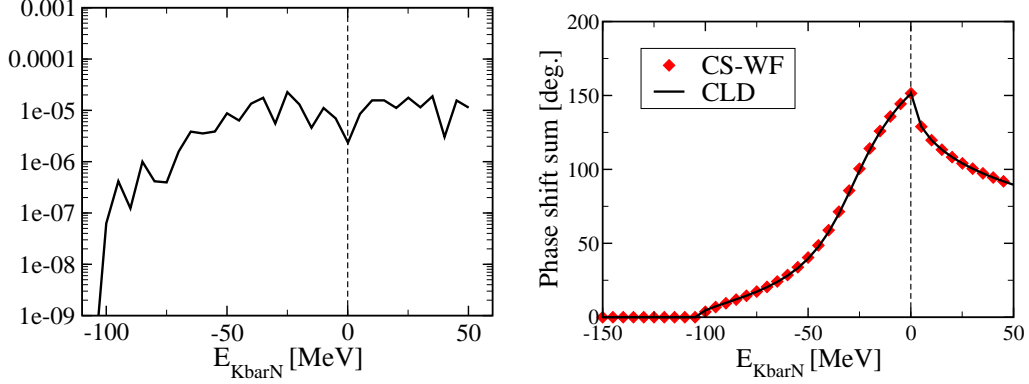


Figure 1: (Left) Unitarity violation of the S -matrix. (Right) Comparison of the phase-shift sum between CS-WF (red diamond) and CLD (black line). “ $E_{K\text{bar}N}$ ” means the energy of the system measured from the $\bar{K}N$ threshold. Here, the $I = 0$ channel is considered.

2.4. Test of $ccCSM$ for scattering amplitude

We test the CS-WF method in $I = 0$ $\bar{K}N$ - $\pi\Sigma$ system, since it is the first time to apply this method to a meson-baryon system. Here, we employ a phenomenological $\bar{K}N$ potential [1] which is a coupled $\bar{K}N$ - $\pi\Sigma$ potential and a local potential with a single Gaussian form in r -space, but an energy-independent potential.

First, we check the unitarity violation of S -matrix; $||\det S| - 1|$. We calculate the S -matrix for the partial wave l with the scattering amplitude obtained by the CS-WF method. The S -matrix element for channels α and β is related to the scattering amplitude as

$$S_{\beta,\alpha}^l = \delta_{\beta,\alpha} + 2ik_\alpha \sqrt{\frac{k_\beta/\mu_\beta}{k_\alpha/\mu_\alpha}} f_{\beta,\alpha}^l, \quad (32)$$

where k_α is the wave number in the channel α . As shown in the left panel of Fig. 1, the magnitude of the unitarity violation is confirmed to be significantly small of the order of 10^{-5} in $\bar{K}N$ energy region of -120 to 30 MeV.

We check also the phase-shift sum. We compare the sum of phase shift, $\delta_{\bar{K}N} + \delta_{\pi\Sigma}$, with that obtained by the continuum level density (CLD) method [28]. Noted that the CLD method can give the phase-shift sum by using eigenvalues of the complex-scaled Hamiltonian, but that it cannot give the phase shift of each channel. Phase shift is obtained from the S -matrix (Eq.

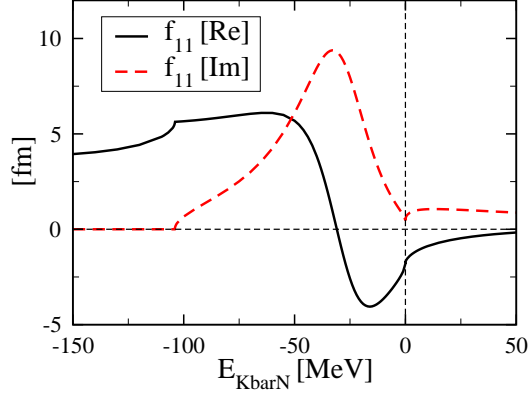


Figure 2: The $\bar{K}N \rightarrow \bar{K}N$ scattering amplitude in the $I = 0$ channel calculated with a phenomenological potential [1].

(32)) as

$$S = \begin{pmatrix} S_{11} & S_{12} \\ S_{21} & S_{22} \end{pmatrix} = \begin{pmatrix} \cos 2\epsilon e^{i\delta_1} & i \sin \epsilon e^{i(\delta_1+\delta_2)} \\ i \sin \epsilon e^{i(\delta_1+\delta_2)} & \cos 2\epsilon e^{i\delta_2} \end{pmatrix}, \quad (33)$$

where δ_i is phase shift of channel i and ϵ is a mixing parameter. As seen in the right panel of Fig. 1, the phase-shift sums calculated with both the methods agree with each other quite well.

We show the $\bar{K}N$ scattering amplitude calculated with our method in Fig. 2. The $\bar{K}N$ scattering amplitude is given in Ref. [1] where it is obtained by solving the Schrödinger equation as usual. Compared them with each other, we find that our calculation reproduces well the original result. (See Fig. 1 in Ref. [1]) The scattering length also coincides well in both calculations: $-1.77 + i0.47$ fm in our calculation and $-1.76 + i0.46$ fm in the original work.

3. Result

We show the results of our calculation with the ccCSM. As mentioned in the section 2.1, the KSW potential and two kinds of non-relativistically approximated one are used, and two kinematics, non-relativistic and semi-relativistic, are examined. Hereafter we abbreviate non-relativistic and semi-relativistic as “NR” and “SR”, respectively. We consider natural combinations of potential types and kinematics as follows:

- Case (i) One of non-relativistic approximated KSW potentials (Eq. (7)), NRv1, with the non-relativistic kinematics.
- Case (ii) The other non-relativistic approximated KSW potentials (Eq. (8)), NRv2, with the non-relativistic kinematics.
- Case (iii) The KSW potential (Eq. (3)) with the semi-relativistic kinematics.

In addition, we investigate an instructive case that the KSW potential is used with the non-relativistic kinematics.

We consider f_π in the KSW potential as a parameter in our model. In the present study, it is varied around the physical values of $f_\pi \simeq 93$ MeV and $f_K \simeq 110$ MeV. We examine four cases of $f_\pi = 90, 100, 110$ and 120 MeV.

3.1. Scattering amplitude of $I = 0$ $\bar{K}N$ - $\pi\Sigma$ system

First, we determine the range parameters of Gaussian functions, $\{d_{\alpha\beta}^{I=0}\}$, in the meson-baryon potentials, Eqs. (3), (7) and (8). In the present study, with an assumption of $d_{\bar{K}N,\pi\Sigma} = d_{\pi\Sigma,\bar{K}N} = (d_{\bar{K}N,\bar{K}N} + d_{\pi\Sigma,\pi\Sigma})/2$, we search for the two of the range parameters, $d_{\bar{K}N,\bar{K}N}$ and $d_{\pi\Sigma,\pi\Sigma}$, so as to reproduce the complex value of $I = 0$ $\bar{K}N$ scattering length which was obtained by Martin's analysis; $a_{\bar{K}N(I=0)} = -1.70 + i0.68$ fm [26]. The range parameters with the calculated $\bar{K}N$ scattering amplitude are listed in Table 1 for $f_\pi = 90$ MeV case. For all combinations of kinematics and meson-baryon potential, we can find the range parameters which reproduce the Martin's value well. Also in cases of $f_\pi = 100, 110$ and 120 MeV, we find such range parameters as given in Table C.6.

Using the meson-baryon potentials with these range parameters, we calculate the scattering amplitude in the $I = 0$ channel. Figs. 3-5 show the $\bar{K}N$ and $\pi\Sigma$ scattering amplitudes for $f_\pi = 90$ MeV. Fig. 3 shows an instructive result where the KSW potential is used in the NR kinematics. As seen in the figure, both the scattering amplitudes behave very singularly near the $\pi\Sigma$ threshold. We consider that such a singular behavior is caused by the mismatch of the kinematics and the potential. Since the flux factor in the KSW potential is relativistic, it should be used under relativistic kinematics. (at least, semi-relativistic one.) Indeed, such a singularity disappears in the cases (i)-(iii) where the potential is used with appropriate kinematics. (See Figs. 4 and 5)

As seen in Figs. 4 and 5, the NR and SR give quantitatively the same $\bar{K}N$ scattering amplitude, though the $\pi\Sigma$ scattering amplitude is different between two kinematics. Let us see the $I = 0$ scattering amplitudes in more

Table 1: Range parameters for $I = 0$ $\bar{K}N$ - $\pi\Sigma$ system. $f_\pi = 90$ MeV case. $d_{\bar{K}N, \bar{K}N}$ ($d_{\pi\Sigma, \pi\Sigma}$) means the range parameter of Gaussian potential in $\bar{K}N$ - $\bar{K}N$ ($\pi\Sigma$ - $\pi\Sigma$) channel. $a_{\bar{K}N(I=0)}$ is the $I = 0$ $\bar{K}N$ scattering length calculated with given range parameters. All quantities are in unit of fm.

Case	—	(i)	(ii)	(iii)
Kinematics		Non-rela.		Semi-rela.
Potential	KSW	NRv1	NRv2	KSW
$d_{\bar{K}N, \bar{K}N}$	0.593	0.576	0.574	0.487
$d_{\pi\Sigma, \pi\Sigma}$	0.541	0.725	0.751	0.457
Re $a_{\bar{K}N(I=0)}$	-1.701	-1.700	-1.700	-1.703
Im $a_{\bar{K}N(I=0)}$	0.679	0.677	0.687	0.677

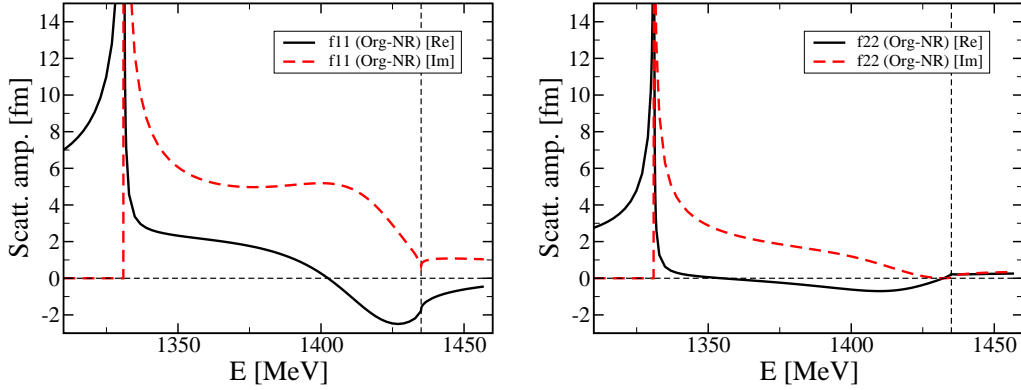


Figure 3: $I = 0$ scattering amplitudes calculated with the original KSW potential and NR kinematics. Left (right) panel shows $\bar{K}N$ ($\pi\Sigma$) scattering amplitude. The real (imaginary) part of scattering amplitude is drawn with a black-solid (red-dashed) line. Vertical dashed line means the $\bar{K}N$ threshold. $f_\pi = 90$ MeV case.

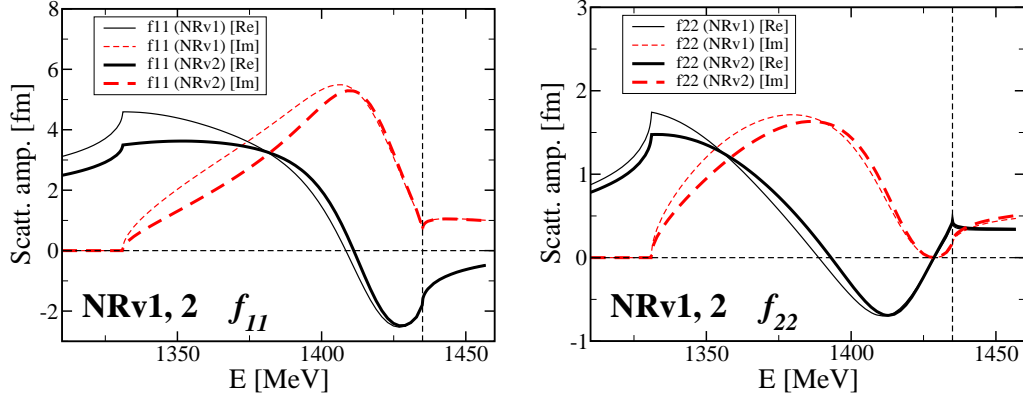


Figure 4: $I = 0$ scattering amplitudes for NRv1 and NRv2 cases. The scattering amplitudes of NRv1 (NRv2) are shown with thin (bold) line. Left (right) panel shows $\bar{K}N$ ($\pi\Sigma$) scattering amplitude. $f_\pi = 90$ MeV case.

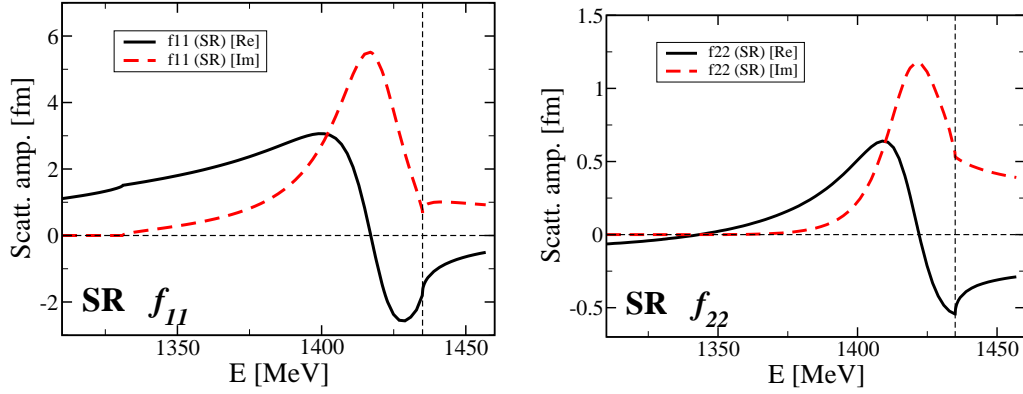


Figure 5: $I = 0$ scattering amplitudes for SR case. Left (right) panel shows $\bar{K}N$ ($\pi\Sigma$) scattering amplitude. $f_\pi = 90$ MeV case.

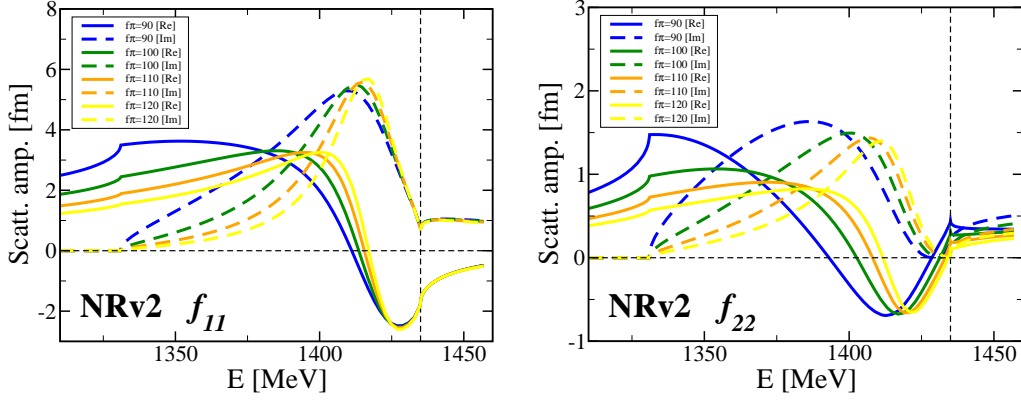


Figure 6: $I = 0$ scattering amplitudes for NRv2 case, calculated with various f_{π} values. Blue, green, orange and yellow lines correspond to $f_{\pi}=90, 100, 110$ and 120 MeV, respectively. Left (right) panel shows $\bar{K}N$ ($\pi\Sigma$) scattering amplitude.

Table 2: Resonant energies estimated from the scattering amplitudes and the $\pi\Sigma$ phase shift. The latter is estimated by $\delta_{\pi\Sigma}(E) = \frac{\pi}{2}$ and $\delta'_{\pi\Sigma}(E) > 0$. $f_{\pi} = 90$ MeV case. The energies are given in unit of MeV.

Case	—	(i)	(ii)	(iii)
Kinematics		Non-rela.		Semi-rela.
Potential	KSW	NRv1	NRv2	KSW
E at $\text{Re } f_{\bar{K}N} = 0$	1402.5	1408.4	1411.1	1417.0
E at $\text{Re } f_{\pi\Sigma} = 0$	1354.6	1388.8	1393.0	1422.0
E at $\delta_{\pi\Sigma} = \frac{\pi}{2}$	1354.6	1388.8	1393.0	1422.0

detail. In two NR cases (i) and (ii), the scattering amplitudes have the same behavior essentially. In the SR case (iii), the real part of the amplitude is smaller in the region far below the $\bar{K}N$ threshold, compared to the NR cases. We investigate the f_{π} dependence of the scattering amplitude. Figs. 6 and 7 are the scattering amplitudes calculated with the NR and SR cases, respectively, when f_{π} is varied from 90 to 120 MeV. In the NR case the scattering amplitude is found to depend strongly on the f_{π} value, especially near the $\pi\Sigma$ threshold. It tends to be less attractive with larger value of f_{π} used. On the other hand, in the SR case, it doesn't depend on the f_{π} value so much.

In all cases, the resonant structure is found in the $\bar{K}N$ and $\pi\Sigma$ scattering amplitudes below the $\bar{K}N$ threshold. The resonant energies estimated from

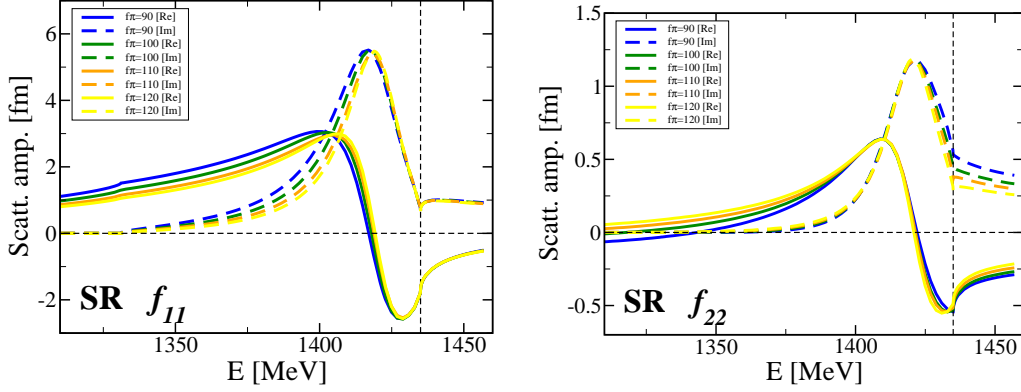


Figure 7: $I = 0$ scattering amplitudes for SR case, calculated with various f_π values. Left (right) panel shows $\bar{K}N$ ($\pi\Sigma$) scattering amplitude.

the scattering amplitude are summarized in Table 2, where they are considered as the energy at which the real part of scattering amplitude becomes zero. The resonant positions on the $\bar{K}N$ scattering amplitude are around 1410 MeV for NR case and near 1420 MeV for SR case. They are rather close to each other. (slightly lower in the NR case compared to the SR case.) On the other hand, on the $\pi\Sigma$ scattering amplitude the resonant positions are rather different between two kinematics: about 1390 MeV in NR whereas about 1420 MeV in SR, for $f_\pi = 90$ MeV. When the f_π value is modified up to 120 MeV, the resonant position on the $\pi\Sigma$ amplitude becomes higher to 1417 MeV in the NR. Compared to the NR case, both the resonant positions on $\bar{K}N$ and $\pi\Sigma$ amplitudes are stable for f_π value in the SR. (See Fig. 8)

3.2. Property of the $I = 0$ $\bar{K}N$ - $\pi\Sigma$ resonant state

Using the meson-baryon potential determined in the previous section, we investigate the resonance in the $I = 0$ $\bar{K}N$ - $\pi\Sigma$ system. In practice, we search poles on the complex energy plane with the usual complex scaling method as explained in the section 2.2.

In all NR and SR cases, one pole is clearly found.² We denote the complex energy of a resonant pole as $(E_R, -\Gamma/2)$. The found poles for the case $f_\pi = 90$ MeV are shown in Table 3. The real part of energy E_R is well determined to

² Preceding studies based on the chiral SU(3) theory reported that there exist two poles in the $I = 0$ channel [17, 18] We will discuss a signature of another pole later.

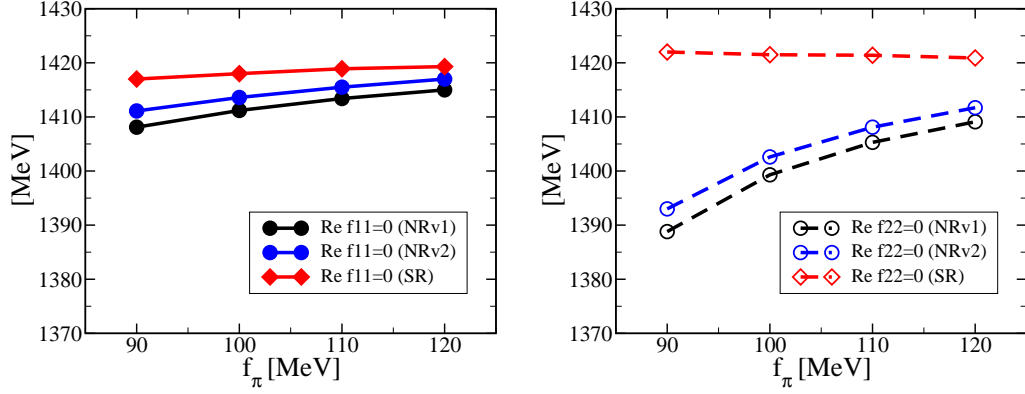


Figure 8: f_π dependence of the resonance position appeared in scattering amplitudes. (Left) obtained from the $\bar{K}N$ scattering amplitude. (Right) obtained from the $\pi\Sigma$ one. A symbol of black (blue) circle means NRv1 (NRv2) and a symbol of red diamond means SR.

Table 3: Pole position of the $I = 0$ $\bar{K}N$ - $\pi\Sigma$ system and the meson-baryon distance in the pole state. $(E_R, -\Gamma/2)$ indicates the complex energy of the resonant pole. $B_{\bar{K}N}$ means the binding energy that is the E_R measured from the $\bar{K}N$ threshold. The unit of these energies is MeV. $\langle\sqrt{r^2}\rangle_{\bar{K}N}$, $\langle\sqrt{r^2}\rangle_{\pi\Sigma}$ and $\langle\sqrt{r^2}\rangle_{\bar{K}N+\pi\Sigma}$ indicate the meson-baryon mean distance of $\bar{K}N$, $\pi\Sigma$ and total components, respectively. These values are given in unit of fm. $f_\pi = 90$ MeV case.

Case	(i)	(ii)	(iii)
Kinematics	Non-rela.		Semi-rela.
Potential	NRv1	NRv2	KSW
E_R	1419.8	1419.9	1419.0
$B_{\bar{K}N}$	15.2	15.1	16.0
$\Gamma/2$	26.0	23.1	14.4
$\sqrt{\langle r^2 \rangle}_{\bar{K}N}$	$1.20 - 0.35i$	$1.25 - 0.35i$	$1.21 - 0.49i$
$\sqrt{\langle r^2 \rangle}_{\pi\Sigma}$	$0.33 + 0.24i$	$0.34 + 0.23i$	$0.12 - 0.09i$
$\sqrt{\langle r^2 \rangle}_{\bar{K}N+\pi\Sigma}$	$1.20 - 0.28i$	$1.25 - 0.29i$	$1.21 - 0.49i$

be about 1420 MeV, independently of kinematics and potential types. The imaginary part of energy $\Gamma/2$ depends on the kinematics; $\Gamma/2 \simeq 14$ MeV in the SR, whereas $\Gamma/2 \simeq 25$ MeV in the NR. Fig. 9 shows the pole positions of all cases when the f_π value is varied from 90 MeV to 120 MeV. In the NR cases, E_R is stable for f_π and is 1417-1420 MeV, but $\Gamma/2$ is ranging from 14 MeV to 26 MeV. In the SR case the poles are found to distribute in compact region. The pole position $(E_R, -\Gamma/2)$ is determined with small deviation; $(1419.5 \pm 1, -13 \pm 2)$ MeV. Thus, in the NR and SR kinematics the real part of energy of the pole is almost identical, though the imaginary one is different between two kinematics. The imaginary part of energy indicates a half width decaying to $\pi\Sigma$. In our study we have a constraint for $\bar{K}N$ channel but no constraint for $\pi\Sigma$ channel. We consider that the difference of $\Gamma/2$ between two kinematics is due to the lack of constraint condition for $\pi\Sigma$ channel.

We have investigated another pole which is expected to exist, because many studies of the $I = 0$ $\bar{K}N$ - $\pi\Sigma$ system reported that this system has a double pole structure when an energy-dependent chiral SU(3) potential is used as we use [17, 18]; The higher pole state is slightly below the $\bar{K}N$ threshold and with small width, while the lower one is far below the $\bar{K}N$ threshold and with large width. (for instance, the former is around (1432, -17) MeV and the latter is around (1400, -80) MeV [18].) In our study, certainly we found self-consistent solutions which seem to indicate a lower pole of the double pole; the complex energy is $(\sim 1360, -40 \sim -90)$ MeV in case of NRv2. However, the separation of the pole from continuum states indicated by the 2θ -line on the complex-energy plane seems insufficient and the pole position, in particular its imaginary energy, rather depends on the scaling angle θ . We consider that this is due to the limitation of the numerical accuracy. When poles have large decay width compared to excitation energy, it is known empirically that such poles are difficult to be found by the CSM with Gaussian base, since the spatial oscillation of the complex-scaled wave function is not well described with them. Therefore, we cannot conclude yet that the double pole structure is confirmed in the present our analysis. We need more investigation of the lower pole.

We are interested in the inertial structure of $\Lambda(1405)$. It has been investigated theoretically in various ways [29, 30, 31]. We consider the wave function of the pole state obtained by our ccCSM calculation. Fig. 10 shows complex-scaled wave functions of each component when the scaling angle $\theta = 30^\circ$. Here, the wave functions are multiplied by an appropriate phase factor so that the $\bar{K}N$ wave function becomes real at $r = 0$. Without this

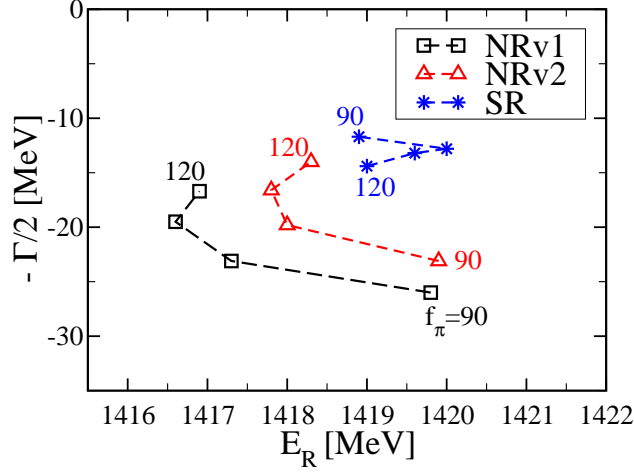


Figure 9: $I = 0$ pole in the complex-energy plane, calculated with NRv1, NRv2, and SR for various f_π values. The number shown in the panel is the f_π value which increases continuously from 90 to 120 along the connected dashed line in each case.

phase factor, the complex-scaled wave function of $\bar{K}N-\pi\Sigma$ is normalized as Eq. (12). Both of $\bar{K}N$ and $\pi\Sigma$ wave functions are confirmed to be well localized. It is noted that localization of the $\pi\Sigma$ component is due to the complex scaling, in spite that the state is above $\pi\Sigma$ threshold.

The mean distance between meson and baryon in the resonant state is calculated as

$$\langle \hat{r}_{MB}^2 \rangle = \langle \tilde{\Phi}_\theta | \hat{r}_{MB,\theta}^2 | \Phi_\theta \rangle, \quad (34)$$

where $\hat{\mathbf{r}}_{MB} = \hat{\mathbf{r}}_{\text{Meson}} - \hat{\mathbf{r}}_{\text{Baryon}}$ and Φ_θ means the complex-scaled wave function of the resonant pole. It should be noted that the matrix elements of resonant state are obtained independently of θ because the properties of the resonant wave functions are uniquely determined in the complex scaling method [32]. The expectation value calculated with Eq. (34) is inevitably a complex number because the resonant state is treated as a Gamow state in our framework. Therefore, the root-mean square distance, $\sqrt{\langle \hat{r}_{MB}^2 \rangle}$, is also a complex number. Certainly its physical meaning is still unclear, but we show this quantity as a reference for the size. We believe that it is useful for us to get a feeling of the size of the system. Indeed, since the imaginary part of the obtained complex mean distance is smaller than its real part as will be shown later, we consider that the real part can be regarded as a mean distance with a physical meaning [32].

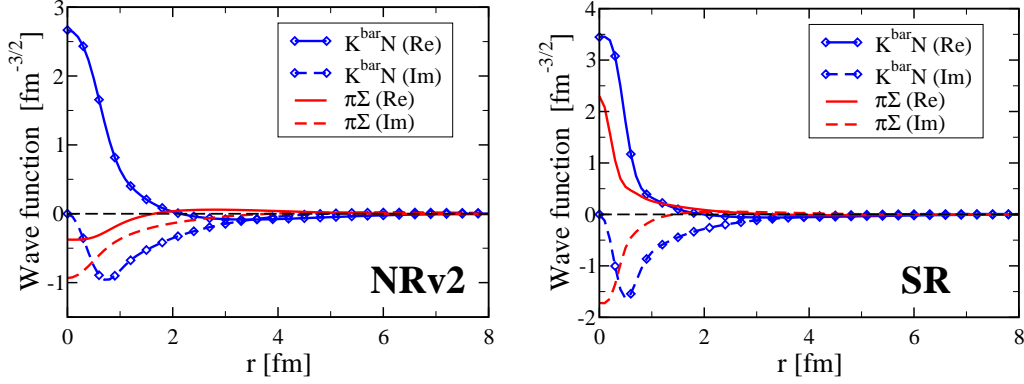


Figure 10: Complex-scaled wave function of each component in the $I = 0$ pole state at $\theta = 30^\circ$. We choose a phase such that the $\bar{K}N$ wave function becomes real at $r = 0$. Left: NRv2, Right: SR. $f_\pi = 90$ MeV case.

If such an interpretation for the complex-valued distance calculated within the ccCSM is accepted, the mean distance between meson and baryon is about 1.2 fm in both cases of NR and SR kinematics with $f_\pi = 90$ MeV, as shown in Table 3. Those for other f_π cases are given in Table C.8. In the SR case the mean distance has small f_π dependence, remaining about 1.2 fm. In the NR case it depends on the f_π value similarly to the pole position, but it increases slightly to be 1.4 fm when f_π is modified to 120 MeV. Thus, it is found that the mean distance is almost the same in both two kinematics. As for the imaginary part of the complex-valued distance, it is certainly small value of 0.5 fm at most.

Compared to results of other studies, the size obtained by our calculation seems rather small, even if the modulus of $\sqrt{\langle \hat{r}_{MB}^2 \rangle}$ is regarded as a mean distance between meson and baryon in the $I = 0$ system. For example, according to a study using a chiral SU(3)-based potential, it is 1.9 fm with 12 MeV binding energy of $\bar{K}N$ ($M = 1423$ MeV) [7]. We think that the difference of size between two calculations is mainly caused by different definition of the resonant state. In the previous study, it is treated as a $\bar{K}N$ bound state, as a result of elimination of $\pi\Sigma$ channel and perturbative treatment of the imaginary part of potential. On the other hand, the resonant state is a Gamow state in the current study since the complex scaling method imposes the outgoing boundary condition on a solution implicitly.

3.3. $I = 1$ $\bar{K}N$ - $\pi\Sigma$ - $\pi\Lambda$ system

We make the same investigation on the isospin $I = 1$ sector which has three channels of $\bar{K}N$, $\pi\Sigma$ and $\pi\Lambda$. In our model of the Gaussian form potential, there are six range parameters in this sector. However, two of them, $d_{\pi\Lambda,\pi\Sigma}$ and $d_{\pi\Lambda,\pi\Lambda}$, give no contribution to the result, since the potential strength of these channels are forced to be zero due to the SU(3) algebra that appears in the lowest-order potential of chiral SU(3) dynamics. (See $C^{(I=1)}$ in Eq. (6)) Since we assume $d_{\bar{K}N,\pi\Sigma} = (d_{\bar{K}N,\bar{K}N} + d_{\pi\Sigma,\pi\Sigma})/2$ similarly to the $I = 0$ case, three range parameters, $d_{\bar{K}N,\bar{K}N}$, $d_{\pi\Sigma,\pi\Sigma}$ and $d_{\bar{K}N,\pi\Lambda}$, are unknown parameters to be determined.

Similarly to the $I = 0$ case, we constrain the range parameters in the potential by the Martin's value of the $I = 1$ $\bar{K}N$ scattering length; $a_{\bar{K}N(I=1)} = 0.37 + i0.60$ fm [26]. However, the three unknown parameters can't be determined by only the complex value of $a_{\bar{K}N(I=1)}$. Here, we reduce the number of unknown parameters by referring the following two facts: 1. In studies with chiral unitary model, isospin symmetric subtraction constants have been often assumed and succeeded to reproduce various physical quantities [33]. 2. In a separable potential used in Faddeev-AGS calculation of $\bar{K}NN$ - πYN [5], the cut off parameter for the $\bar{K}N$ channel is not so different between $I = 0$ and $I = 1$ sector. Based on these facts, we examine three conditions as follows:

- Cond. (a) $d_{\bar{K}N,\bar{K}N}$ is fixed to that of the $I = 0$ case.
 $d_{\pi\Sigma,\pi\Sigma}$ and $d_{\bar{K}N,\pi\Lambda}$ are searched to reproduce the complex value of $a_{\bar{K}N(I=1)}$.
- Cond. (b) $d_{\bar{K}N,\bar{K}N}$ and $d_{\pi\Sigma,\pi\Sigma}$ are fixed to those of the $I = 0$ case.
 $d_{\bar{K}N,\pi\Lambda}$ is searched to reproduce the real part of $a_{\bar{K}N(I=1)}$.
- Cond. (c) Similar to the condition (b), but $d_{\bar{K}N,\pi\Lambda}$ is searched to reproduce the imaginary part of $a_{\bar{K}N(I=1)}$.

We describe mainly the result with $f_\pi = 90$ MeV. In the NR case, we can find a set of range parameters which satisfy each condition (a)-(c), as shown in Table 4. However, it is found that the $I = 1$ scattering amplitude calculated with the condition (a) has a resonant structure slightly below $\pi\Sigma$ threshold as shown in the left column of Fig. 11,³ although no resonance in $I = 1$ sector has been confirmed theoretically and experimentally. In the

³In this case we have found a pole on the complex-energy plane by the ccCSM at $(E_R, -\Gamma/2) = (1326.4, -1.3)$ MeV. Certainly, this pole exists only by 5 MeV below $\pi\Sigma$ threshold (=1331 MeV).

Table 4: Range parameters for the $I = 1$ $\bar{K}N$ - $\pi\Sigma$ - $\pi\Lambda$ system with the non-relativistic kinematics. $f_\pi = 90$ MeV case. The same table as that in Table 1. “Condition” is explained in the text.

Case	(i)			(ii)		
Kinematics	Non-rela.			Non-rela.		
Potential	NRv1			NRv2		
Condition	(a)	(b)	(c)	(a)	(b)	(c)
$d_{\bar{K}N, \bar{K}N}$	0.576	0.576	0.576	0.574	0.574	0.574
$d_{\pi\Sigma, \pi\Sigma}$	0.212	0.725	0.725	0.221	0.751	0.751
$d_{\bar{K}N, \pi\Lambda}$	0.355	0.502	1.038	0.391	0.558	1.138
Re $a_{\bar{K}N(I=1)}$	0.372	0.371	0.650	0.371	0.370	0.621
Im $a_{\bar{K}N(I=1)}$	0.601	1.444	0.600	0.601	1.358	0.600

conditions (b) and (c), such a resonant structure does not appear in all the scattering amplitudes. (See the right column of Fig. 11)

In the SR case, a set of range parameters to satisfy the conditions is found only in the case (a), but is not found in the cases (b) and (c). (See the left three columns in Table 5) Scattering amplitudes calculated with the range parameters of the condition (a) is shown in the left column of Fig. 12. As seen in this figure, the $\pi\Sigma$ scattering amplitude indicates repulsive nature of $\pi\Sigma$ - $\pi\Sigma$ channel, in spite that the direct $\pi\Sigma$ potential is originally attractive. This is considered to be a consequence of the coupled-channel effect.

We investigate other f_π values such as 100, 110 and 120 MeV. Range parameters and $\bar{K}N$ scattering length for these f_π ’s are listed in Table C.9. It is confirmed that the scattering amplitudes for these f_π ’s are essentially the same as those for $f_\pi = 90$ MeV case above mentioned.

We consider the cases where the conditions are slightly relaxed. First, we vary the value of the range parameter $d_{\bar{K}N, \bar{K}N}$ slightly in the condition (a), since it may be too strict constraint that $d_{\bar{K}N, \bar{K}N}$ is fixed to that of the $I = 0$ sector. With 10% modification of the $d_{\bar{K}N, \bar{K}N}$, essential property of the scattering amplitude is found to be unchanged; In the SR the $\pi\Sigma$ scattering amplitude still indicates the repulsive nature, and in the NR a resonant structure is kept to appear around the $\pi\Sigma$ threshold. Next, we consider a case that only the imaginary part of $a_{\bar{K}N(I=1)}$ is reproduced in the condition (a) with the SR case, giving up the reproduction of its real

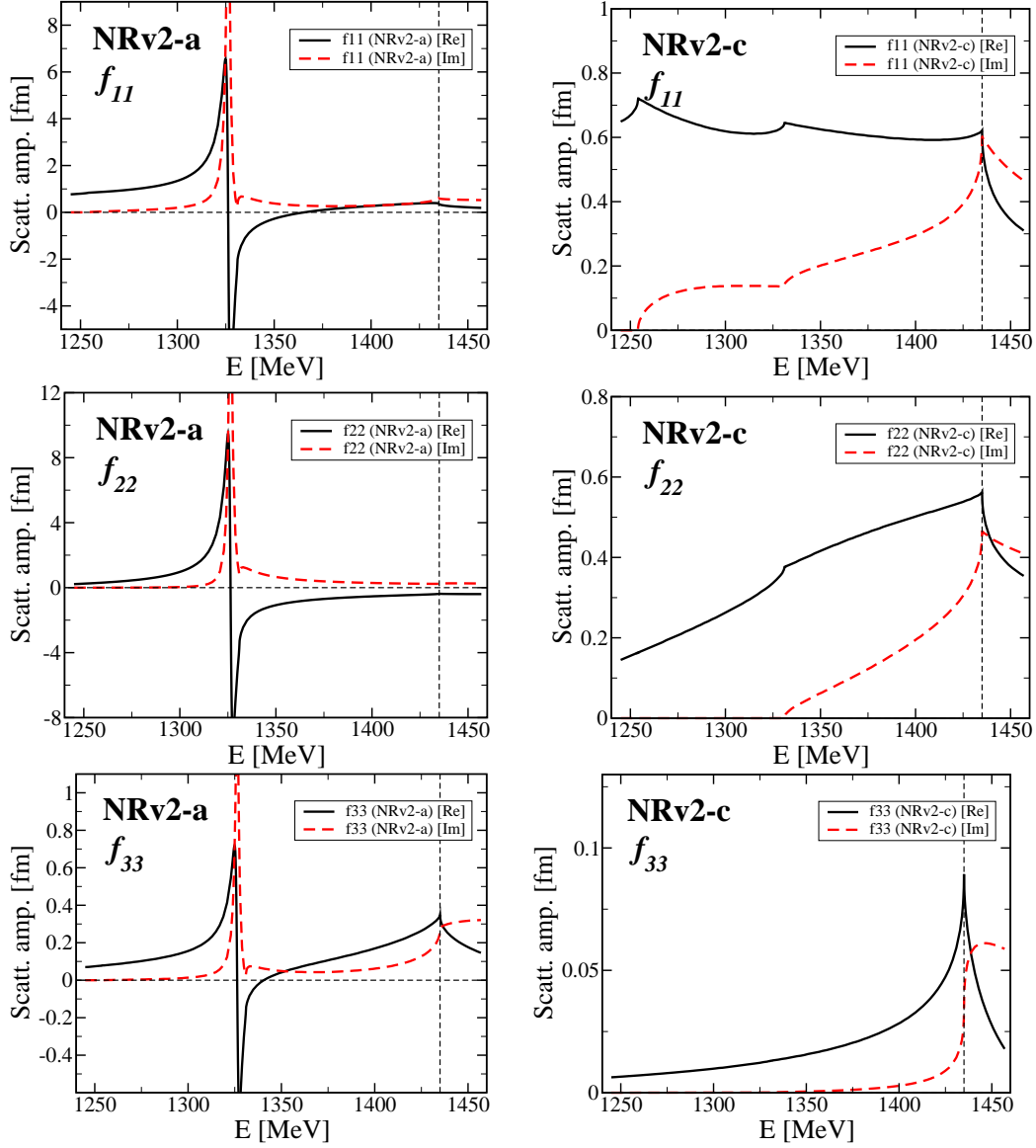


Figure 11: $I = 1$ scattering amplitude calculated with NRv2. Left (Right) panels are calculated with the condition (a) (condition (c)). Top: $\bar{K}N \rightarrow \bar{K}N$, Middle: $\pi\Sigma \rightarrow \pi\Sigma$, Bottom: $\pi\Lambda \rightarrow \pi\Lambda$. $f_\pi = 90$ MeV case.

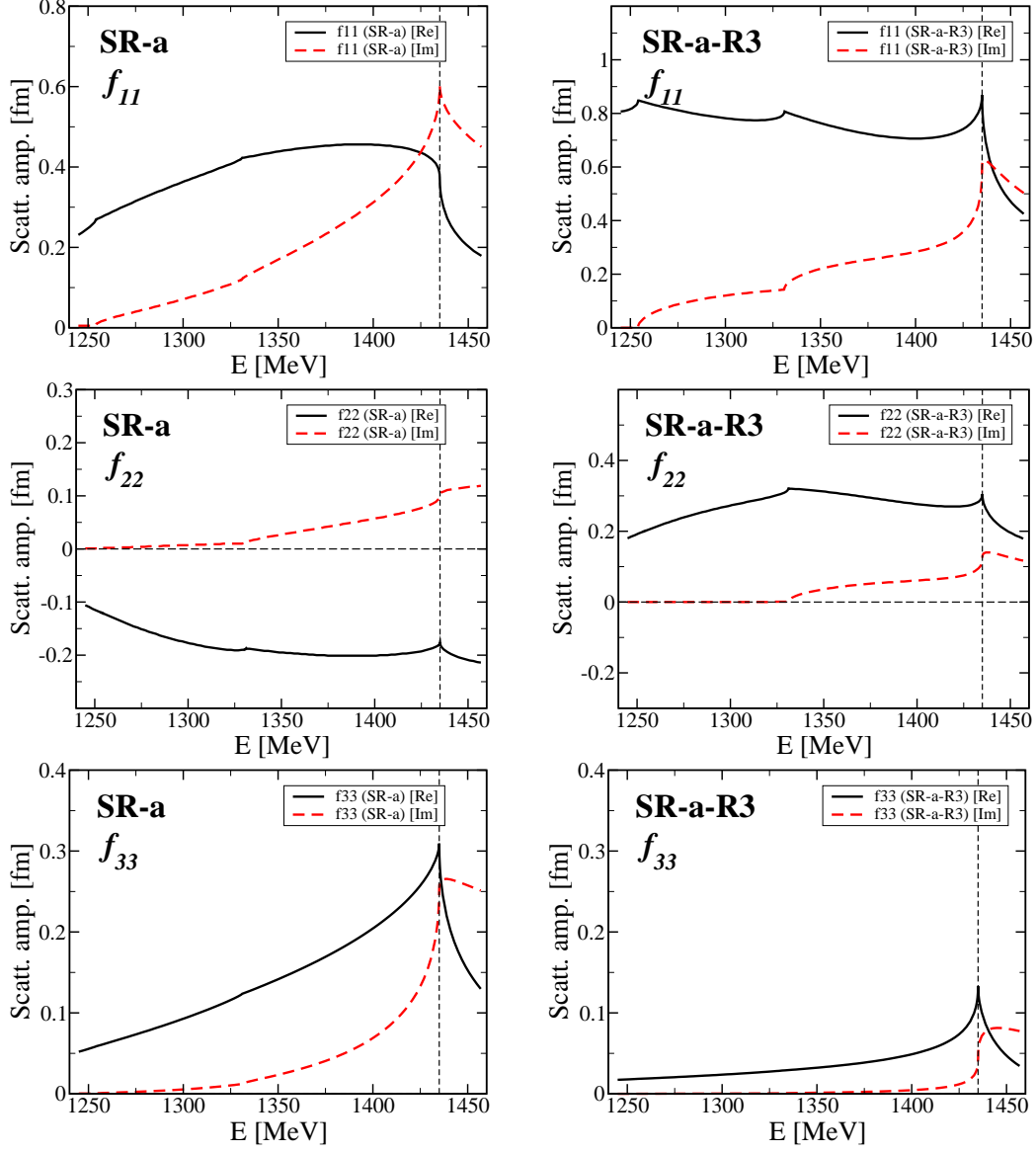


Figure 12: $I = 1$ scattering amplitude calculated with SR. Left (Right) panels are calculated with the condition (a) (condition (a)-R3). Top: $\bar{K}N \rightarrow \bar{K}N$, Middle: $\pi\Sigma \rightarrow \pi\Sigma$, Bottom: $\pi\Lambda \rightarrow \pi\Lambda$. $f_\pi = 90$ MeV case.

Table 5: Range parameters for the $I = 1$ $\bar{K}N$ - $\pi\Sigma$ - $\pi\Lambda$ system with the semi-relativistic kinematics. $f_\pi = 90$ MeV case. Columns “(a)-R1” to “(a)-R3” show the results obtained with the condition (a) relaxed. Details are explained in the text.

Case	(iii)			(iii)		
Kinematics	Semi-rela.			Semi-rela.		
Potential	KSW			KSW		
Condition	(a)	(b)	(c)	(a)-R1	(a)-R2	(a)-R3
$d_{\bar{K}N, \bar{K}N}$	0.487	0.487	0.487	0.487	0.487	0.487
$d_{\pi\Sigma, \pi\Sigma}$	0.313	0.457	0.457	0.960	1.210	1.340
$d_{\bar{K}N, \pi\Lambda}$	0.422	0.187	0.100	1.550	1.000	0.930
Re $a_{\bar{K}N(I=1)}$	0.374	0.072	-0.145	0.932	0.871	0.869
Im $a_{\bar{K}N(I=1)}$	0.602	0.268	0.404	0.591	0.600	0.600

part. We can obtain some sets of range parameters satisfying such a relaxed condition (a) as listed on the right three columns in Table 5. When these range parameters are used, the $\pi\Sigma$ scattering amplitude is found to indicate attractive nature as seen in the right column of Fig. 12. Compared with the NR result shown in the right column of Fig. 11 (NRv2-c), it is noticed that the SR and NR give quite a similar result for all channels of $\bar{K}N$, $\pi\Sigma$ and $\pi\Lambda$, in such a case that Im $a_{\bar{K}N(I=1)}$ is fixed to be the experimental value.

4. Summary and future plan

We have studied a $\bar{K}N$ - πY system with a coupled-channel complex scaling method (ccCSM) [23] using a chiral SU(3) potential. In our study, scattering states as well as resonant states are investigated within a single framework of ccCSM. Resonant poles are obtained by diagonalizing a complex-scaled Hamiltonian with Gaussian base, similarly to bound states calculation. Scattering problem is solved with an advanced use of ccCSM, “CS-WF” method [25]. In the CS-WF, due to Cauchy’s theorem scattering amplitudes are calculated with a complex-scaled wave function which is also described with Gaussian base. Thus, both of resonant and scattering problems can be solved with Gaussian base and therefore they can be treated with small modification of bound-state calculation. This is the most advantageous point of ccCSM.

Based on Ref. [14] where a meson-baryon potential is derived from a chiral SU(3) theory, we have constructed a meson-baryon potential (KSW potential) which is a local potential with Gaussian form in r -space. Since in the present study it is necessary to deal with pion whose mass is very light, we have examined semi-relativistic kinematics (SR) as well as non-relativistic one (NR). In the NR case, non-relativistically approximated versions of the KSW potential are used.

By using the CS-WF method, range parameters of our Gaussian-form potential are determined for both the NR and SR kinematics, so as to reproduce the value of $\bar{K}N$ scattering length obtained by Martin's analysis [26]. The scattering amplitudes are investigated with the CS-WF method using the determined potentials.

In the $I = 0$ sector, it is found that the $\bar{K}N$ scattering amplitude near the $\bar{K}N$ threshold is well constrained by the $\bar{K}N$ scattering length, since its f_π dependence is small and both kinematics give similar results. However, far below the $\bar{K}N$ threshold the scattering amplitudes are strongly dependent on the f_π value in NR and the results of NR and SR are rather different from each other. We consider that further data far below $\bar{K}N$ threshold, such as $\pi\Sigma$ scattering length, are necessary to reduce such an uncertainty in the deep $\bar{K}N$ bound region, as pointed out in Ref. [34]. A resonant structure is seen below the $\bar{K}N$ threshold in the $I = 0$ $\bar{K}N$ and $\pi\Sigma$ scattering amplitudes. For the modification of the f_π value, it is confirmed that in the NR case the resonant position of $\pi\Sigma$ scattering amplitude is rather varied, whereas in the SR case it is quite stable around 1420 MeV in both of $\bar{K}N$ and $\pi\Sigma$ scattering amplitudes.

Similarly, the $I = 1$ sector has also been investigated. When the potential of our model is constrained by the complex value of $I = 1$ $\bar{K}N$ scattering length, it is found that the scattering amplitude has a resonant structure slightly below the $\pi\Sigma$ threshold in the NR case, and that $\pi\Sigma$ scattering amplitude shows repulsive nature in the SR case. However, if the constraint condition for the potential is relaxed so that only the imaginary part of the $\bar{K}N$ scattering length is reproduced, such a resonant structure disappears in the NR case and the $\pi\Sigma$ scattering amplitude becomes attractive in the SR case.

Property of the resonant pole in the $I = 0$ sector corresponding to the $\Lambda(1405)$ has been studied with the usual ccCSM. For $f_\pi = 90 \sim 120$ MeV,

resonance pole is found around

$$(E_R, -\Gamma/2) = \begin{cases} (1418.5 \pm 1.5, -19.5 \pm 5.5) & \text{in NR case,} \\ (1419 \pm 1, -13 \pm 2) & \text{in SR case,} \end{cases}$$

on the complex energy plane. In the NR case, imaginary part of the pole energy is rather dependent on the f_π value, while in the SR case, both real and imaginary parts of the pole energy are quite stable for the f_π value. As well as the pole energy, it is found that the f_π dependence of various quantities is small in the SR calculation rather than in the NR one. We have estimated the “size” of the pole state by evaluating a root-mean distance with a bi-orthogonal set of complex-scaled wave function, $\sqrt{\langle \hat{r}_{MB}^2 \rangle}$. This quantity does not mean the physical meson-baryon distance since it is natural to be a complex value, but is expected to give us a guide of mean distance. The calculated meson-baryon “distance”s are similar value for the NR and SR cases; $1.3 - i0.3$ fm for the NR case and $1.2 - i0.5$ fm for the SR case.

As a result of the current study with the NR and SR kinematics, it is found that both the kinematics give essentially the same result on $\bar{K}N$ quantities such as the $\bar{K}N$ scattering amplitude, the real energy of $I = 0$ pole state and its size, when we constrain the model by the $\bar{K}N$ scattering length that is the quantity at the threshold. However, difference between them becomes large as for the quantities far below the $\bar{K}N$ threshold and those related to $\pi\Sigma$, where the relativistic effect becomes important.

The pole above discussed is considered to be the higher pole of the double pole of $\Lambda(1405)$. As mentioned in the section 3.2, we found a signature of the lower pole around ($\sim 1360, -40 \sim -90$) MeV in a non-relativistic case. However, we can’t conclude that this is the lower pole, because its θ trajectory is somehow unstable. We think that this is due to limitation of numerical accuracy of the CSM with Gaussian base for the case of large decay width. The poles of broad resonances can be investigated by applying an analytic continuation in the coupling constant to the complex scaling method (ACCC+CSM) [35]. It is one of our future plans to carry out ACCC+CSM and clarify whether our potential leads to the double-pole structure or not.

Thus, we have a $\bar{K}N$ - πY potential for both isospin channels, which is based on a chiral SU(3) theory and is a local Gaussian form in r -space. In our future plan, we will investigate the three-body system of K^-pp ($\bar{K}NN$ - πYN system with $J^\pi = 0^-, T = 1/2$) which is the most essential kaonic nuclei. Since the ccCSM can adequately deal with resonant states of a multi-channel system in principle and the CSM is known to be effective for the nuclear

many-body study [24], we expect that the ccCSM will give a pole position of the K^-pp accurately and reveal its structure. We have interested in the role of πYN three-body dynamics, because its implicit/explicit treatment may cause a large difference in the binding of K^-pp as pointed out in Ref. [36]. It is expected that the contribution of πYN three-body dynamics will be investigated with the ccCSM.

We think that it is worthwhile to use the updated value of the $\bar{K}N$ scattering length, instead of the Martin's value obtained from old data, in our analysis. The SIDDHARTA group reported the K^-p scattering length directly from the precise measurement of the shift and width of the $1s$ atomic level energy of kaonic hydrogen atom [20]. Using this data, the K^-n scattering length is estimated with the coupled-channel chiral dynamics [22]. These values of K^-p and K^-n scattering lengths are available in our calculation. Furthermore, the SIDDHARTA group is planning to perform experiments on kaonic deuterium in the SIDDHARTA-2 experiment. These forthcoming experiment will provide us the more precise values of $\bar{K}N$ scattering length for both isospin channels [37].

Furthermore, the ccCSM approach can be applied to other hadronic systems. For instance, it seems interesting to investigate with this method a few-body system involving D meson in the charm sector, which is an analogous system with \bar{K} meson in the strangeness sector [38].

Acknowledgment

One of authors (A. D.) is thankful to Prof. Kato for his advice on the scattering-amplitude calculation based on the complex scaling method, and to Dr. Hyodo for fruitful discussion on the $\bar{K}N$ system. He is grateful also to Prof. Oset and Prof. Gal for their useful comments to improve our paper.

Appendix A. Scattering amplitude for a multi-channel case

We consider a Schrödinger equation for a multi-channel system; $H|\Psi\rangle = E|\Psi\rangle$. Hamiltonian H and total wave function $|\Psi\rangle$ are given as

$$H = \sum_c H_c^0 |c\rangle\langle c| + \sum_{c,c'} V_{cc'} |c\rangle\langle c'|, \quad |\Psi\rangle = \sum_c |\Psi_c\rangle |c\rangle, \quad (\text{A.1})$$

where H_c^0 is the kinetic energy operator $\mathbf{p}_c^2/2\mu_c$ for the channel c and $V_{cc'}$ is a potential between channels c and c' . $|\Psi_c\rangle$ is a wave function of a channel

c . Projecting the Schrödinger equation onto a channel c , we get such an equation for the c -channel wave function as

$$H_c^0 |\Psi_c\rangle + \sum_{c'} V_{cc'} |\Psi_{c'}\rangle = E |\Psi_c\rangle. \quad (\text{A.2})$$

When the incident channel is c_0 and the incoming wave function is given as $|\phi_{c_0, \mathbf{k}_{c_0}}\rangle$, the above equation can be modified formally as

$$|\Psi_c^{(c_0)}\rangle = |\phi_{c_0, \mathbf{k}_{c_0}}\rangle \delta_{cc_0} + \frac{1}{E - H_c^0 + i\epsilon} \sum_{c'} V_{cc'} |\Psi_{c'}^{(c_0)}\rangle, \quad (\text{A.3})$$

taking into account the outgoing boundary condition appropriately. Here, we write the incoming channel c_0 on the wave function of each channel explicitly. The above equation is expressed in r -space as

$$\begin{aligned} \Psi_c^{(c_0)}(\mathbf{r}_c) &= \phi_{c_0, \mathbf{k}_{c_0}}(\mathbf{r}_{c_0}) \delta_{cc_0} \\ &+ \sum_{c'} \int d\mathbf{r}'_c G_c(\mathbf{r}_c, \mathbf{r}'_c; E) \langle \mathbf{r}'_c | V_{cc'} | \Psi_{c'}^{(c_0)} \rangle, \end{aligned} \quad (\text{A.4})$$

where $G_c(\mathbf{r}_c, \mathbf{r}'_c; E)$ is a Green function in the channel c . By performing complex integral as shown in many textbooks, it becomes

$$G_c(\mathbf{r}_c, \mathbf{r}'_c; E) = \langle \mathbf{r}_c | \frac{1}{E - H_c^0 + i\epsilon} | \mathbf{r}'_c \rangle = -\frac{1}{4\pi} \frac{2\mu_c}{\hbar^2} \frac{e^{ik_c |\mathbf{r}_c - \mathbf{r}'_c|}}{|\mathbf{r}_c - \mathbf{r}'_c|} \quad (\text{A.5})$$

$$\simeq -\frac{1}{4\pi} \frac{2\mu_c}{\hbar^2} \frac{e^{ik_c r_c}}{r_c} e^{-i\mathbf{k}_c \cdot \mathbf{r}'_c} \quad (|\mathbf{r}_c| \gg |\mathbf{r}'_c|), \quad (\text{A.6})$$

where $\mathbf{k}_c = k_c \mathbf{r}_c / r_c$ and $r_c = |\mathbf{r}_c|$. Then, the channel- c wave function becomes

$$\Psi_c^{(c_0)}(\mathbf{r}_c) = \phi_{c_0}(\mathbf{r}_{c_0}) \delta_{cc_0} + \frac{e^{ik_c r_c}}{r_c} \times \left(-\frac{1}{4\pi} \right) \frac{2\mu_c}{\hbar^2} \sum_{c'} \langle \phi_{c, \mathbf{k}_c} | V_{cc'} | \Psi_{c'}^{(c_0)} \rangle, \quad (\text{A.7})$$

using the fact that the function $\phi_{c, \mathbf{k}_c}(\mathbf{r}_c)$ is $e^{i\mathbf{k}_c \cdot \mathbf{r}_c}$. Substituting the channel- c wave function in Eq. (A.1) with the above expression, the total wave function is given as

$$|\Psi\rangle = \phi_{c_0}(\mathbf{r}_{c_0}) |c_0\rangle + \sum_c \frac{e^{ik_c r_c}}{r_c} |c\rangle \cdot \left(-\frac{1}{4\pi} \right) \frac{2\mu_c}{\hbar^2} \sum_{c'} \langle \phi_{c, \mathbf{k}_c} | V_{cc'} | \Psi_{c'}^{(c_0)} \rangle. \quad (\text{A.8})$$

Therefore, the scattering amplitude between the initial channel c_0 and the final channel c is

$$f_{cc_0}(\mathbf{k}_c, \mathbf{k}_{c_0}) = -\frac{1}{4\pi} \frac{2\mu_c}{\hbar^2} \sum_{c'} \langle \phi_{c, \mathbf{k}_c} | V_{cc'} | \Psi_{c'}^{(c_0)} \rangle. \quad (\text{A.9})$$

The wave functions $\phi_{c, \mathbf{k}_c}(\mathbf{r}) = e^{i\mathbf{k}_c \cdot \mathbf{r}}$ and $\Psi_{c'}^{(c_0)}(\mathbf{r})$ are expanded on partial waves l as

$$\phi_{c, \mathbf{k}_c}(\mathbf{r}) = 4\pi \sum_{l, m} i^l \frac{\hat{j}_l(k_c r)}{k_c r} Y_{lm}^*(\Omega_{\mathbf{k}_c}) Y_{lm}(\Omega_{\mathbf{r}}), \quad (\text{A.10})$$

$$\Psi_{c'}^{(c_0)}(\mathbf{r}) = 4\pi \sum_{l, m} i^l \frac{\psi_{l, c'}^{(c_0)}(r)}{k_{c_0} r} Y_{lm}^*(\Omega_{\mathbf{k}_{c_0}}) Y_{lm}(\Omega_{\mathbf{r}}) \quad (\text{A.11})$$

and the scattering amplitude is expanded on the orbital angular momentum as

$$f_{cc_0}(\mathbf{k}_c, \mathbf{k}_{c_0}) = \sum_l (2l+1) P_l(\cos \theta(\mathbf{k}_c, \mathbf{k}_{c_0})) f_{l, cc_0}(k_c, k_{c_0}). \quad (\text{A.12})$$

Thus, expanding Eq. (A.9) for the partial waves using Eqs. (A.10)-(A.12), the scattering amplitude for the partial wave l is given as

$$f_{l, cc_0}(k_c, k_{c_0}) = -\frac{2\mu_c}{\hbar^2 k_c k_{c_0}} \sum_{c'} \langle \hat{j}_l(k_c r) | V_{cc'} | \psi_{l, c'}^{(c_0)}(r) \rangle, \quad (\text{A.13})$$

if the potential $V_{cc'}$ is a central potential.

Appendix B. Matrix element of the kinetic term in the semi-relativistic case

In the semi-relativistic kinematics, the kinetic energy and mass terms in the Hamiltonian are of the form of $\sqrt{m^2 + \hat{\mathbf{p}}^2} + \sqrt{M^2 + \hat{\mathbf{p}}^2}$ as shown in Eq. (2). In this article, a wave function is expanded in terms of partial waves; $\Psi(\mathbf{r}) = \sum_{lm} r^{-1} \psi_l(r) Y_{lm}(\Omega)$. Furthermore its radial part is expanded with a Gaussian base, as Eq.(14) and Eq.(24) explained in non-relativistic case;

$$\psi_l(r)/r = \sum_j C_j^l G_j^l(r)/r, \quad G_j^l(r) = N_l(b_j) r^{l+1} \exp[-r^2/2b_j^2], \quad (\text{B.1})$$

where $N_l(b_j)$ means a normalization factor. We need to calculate the matrix element $\langle r^{-1}G_i^l Y_{lm} | \sqrt{m^2 + \hat{\mathbf{p}}^2} | r^{-1}G_j^{l'} Y_{l'm'} \rangle$. This matrix element is calculated as follows:

$$\begin{aligned}
& \langle \frac{1}{r} G_i^l Y_{lm} | \sqrt{m^2 + \hat{\mathbf{p}}^2} | \frac{1}{r} G_j^{l'} Y_{l'm'} \rangle \\
&= \int d\mathbf{r} d\mathbf{r}' d\mathbf{q} d\mathbf{q}' \langle \frac{1}{r} G_i^l Y_{lm} | \mathbf{r} \rangle \langle \mathbf{r} | \mathbf{q} \rangle \langle \mathbf{q} | \sqrt{m^2 + \hat{\mathbf{p}}^2} | \mathbf{q}' \rangle \langle \mathbf{q}' | \mathbf{r}' \rangle \langle \mathbf{r}' | \frac{1}{r'} G_j^{l'} \rangle \\
&= \delta_{ll'} \delta_{mm'} \frac{2}{\pi} \int_0^\infty dq q^2 \sqrt{m^2 + q^2} \\
&\quad \times \int_0^\infty dr G_i^l(r) j_l(qr) \times \int_0^\infty dr' G_j^{l'}(r') j_l(qr'), \quad (\text{B.2})
\end{aligned}$$

where $\langle \mathbf{r} | \mathbf{q} \rangle = e^{i\mathbf{q}\cdot\mathbf{r}}$ and its expansion (Eq. (A.10)) is used. In case of s -wave ($l = 0$) which we are considering in this article, the last integration for r and r' variables can be performed analytically. Finally, the above matrix element for a complex-scaled $\hat{\mathbf{p}}$ is expressed as

$$\begin{aligned}
& \langle \frac{1}{r} G_i^0 Y_{00} | \sqrt{m^2 + (\hat{\mathbf{p}} e^{-i\theta})^2} | \frac{1}{r} G_j^0 Y_{00} \rangle \\
&= \frac{4}{\sqrt{\pi}} (b_i b_j)^{3/2} \int_0^\infty dq q^2 \sqrt{m^2 + q^2} e^{-2i\theta} \exp \left[-\frac{1}{2} (b_i^2 + b_j^2) q^2 \right]. \quad (\text{B.3})
\end{aligned}$$

The integration for the variable q is carried out numerically. The matrix element of Eq. (B.3) is used when we diagonalize the complex-scaled Hamiltonian to find resonant poles as explained in section 2.2 and we calculate a complex-scaled wave function as shown in Eq. (25) to obtain scattering amplitudes.

Note that in a semi-relativistic case any wave number k is calculated from $\sqrt{m^2 + \hbar k^2} + \sqrt{M^2 + \hbar k^2} = E$ and that any reduced mass μ in a non-relativistic case is replaced with corresponding reduced energy $\omega = E_M E_B / (E_M + E_B)$ where E_M and E_B mean meson and baryon energies, respectively; $E_M = \sqrt{m^2 + \hbar k^2}$ and $E_B = \sqrt{M^2 + \hbar k^2}$.

Appendix C. Detailed results of $f_\pi = 100, 110, 120$ MeV cases

We show the results for the cases of $f_\pi = 100, 110$ and 120 MeV. Tables C.6, C.7 and C.8 correspond to Tables 1, 2 and 3 which are for the case of $f_\pi = 90$ MeV, respectively. Table C.9 shows the result corresponding to the case (ii) in Table 4 and the cases (iii)-(a) to (c) in Table 5.

Table C.6: Range parameters for $I = 0$ $\bar{K}N$ - $\pi\Sigma$ system. All quantities are in unit of fm. $f_\pi = 100, 110$ and 120 MeV cases. Corresponding to Table 1.

Case	(i)	(ii)	(iii)
Kinematics	Non-rela.		Semi-rela.
Potential	NRv1	NRv2	KSW
$f_\pi = 100$			
$d_{\bar{K}N, \bar{K}N}$	0.503	0.501	0.421
$d_{\pi\Sigma, \pi\Sigma}$	0.665	0.695	0.395
Re $a_{\bar{K}N(I=0)}$	-1.702	-1.702	-1.703
Im $a_{\bar{K}N(I=0)}$	0.680	0.683	0.673
$f_\pi = 110$			
$d_{\bar{K}N, \bar{K}N}$	0.440	0.438	0.369
$d_{\pi\Sigma, \pi\Sigma}$	0.605	0.636	0.348
Re $a_{\bar{K}N(I=0)}$	-1.701	-1.700	-1.696
Im $a_{\bar{K}N(I=0)}$	0.681	0.681	0.681
$f_\pi = 120$			
$d_{\bar{K}N, \bar{K}N}$	0.386	0.384	0.327
$d_{\pi\Sigma, \pi\Sigma}$	0.549	0.581	0.310
Re $a_{\bar{K}N(I=0)}$	-1.699	-1.700	-1.690
Im $a_{\bar{K}N(I=0)}$	0.674	0.669	0.669

References

- [1] Y. Akaishi and T. Yamazaki, Phys. Rev. C **65**, 044005 (2002); T. Yamazaki and Y. Akaishi, Phys. Lett. B **535**, 70 (2002).
- [2] A. Doté, H. Horiuchi, Y. Akaishi and T. Yamazaki, Phys. Lett. B **590**, 51 (2004); Phys. Rev. C **70**, 044313 (2004).
- [3] D. Gazda, E. Friedman, A. Gal and J. Mares, Phys. Rev. C **76**, 055204 (2007); Phys. Rev. C **77**, 045206 (2008). A. Cieply, E. Friedman, A. Gal, D. Gazda and J. Mares, Phys. Rev. C **84**, 045206 (2011).
- [4] T. Muto, T. Maruyama and T. Tatsumi, Phys. Rev. C **79**, 035207 (2009).
- [5] Y. Ikeda and T. Sato, Phys. Rev. C **76**, 035203 (2007).

Table C.7: Energy of the resonant structure appeared in the scattering amplitude and the $\pi\Sigma$ phase shift. $f_\pi = 100, 110$ and 120 MeV cases. Corresponding to Table 2.

Case	(i)	(ii)	(iii)
Kinematics	Non-rela.		Semi-rela.
Potential	NRv1	NRv2	KSW
$f_\pi = 100$			
E at $\text{Re } f_{\bar{K}N} = 0$	1411.2	1413.6	1418.0
E at $\text{Re } f_{\pi\Sigma} = 0$	1399.3	1402.6	1421.5
$f_\pi = 110$			
E at $\text{Re } f_{\bar{K}N} = 0$	1413.4	1415.5	1418.9
E at $\text{Re } f_{\pi\Sigma} = 0$	1405.3	1408.1	1421.4
$f_\pi = 120$			
E at $\text{Re } f_{\bar{K}N} = 0$	1415.0	1417.0	1419.3
E at $\text{Re } f_{\pi\Sigma} = 0$	1409.1	1411.7	1420.9

- [6] N. V. Shevchenko, A. Gal, J. Mares, and J. Révai, Phys. Rev. C **76**, 044004 (2007).
- [7] A. Doté, T. Hyodo and W. Weise, Nucl. Phys. A **804**, 197 (2008); Phys. Rev. C **79**, 014003 (2009).
- [8] S. Wycech and A. M. Green, Phys. Rev. C **79**, 014001 (2009).
- [9] A. Gal, Prog. Theor. Phys. Suppl. **186**, 270 (2010).
- [10] M. Agnello *et al.* (FINUDA collaboration), Phys. Rev. Lett. **94**, 212303 (2005).
- [11] T. Yamazaki *et al.* (DISTO collaboration), Phys. Rev. Lett. **104**, 132502 (2010).
- [12] V. K. Magas, E. Oset, A. Ramos and H. Toki, Phys. Rev. C **74**, 025206 (2006).
- [13] N. Isgur and G. Karl, Phys. Rev. D **18**, 4187 (1978).
- [14] N. Kaiser, P. B. Siegel and W. Weise, Nucl. Phys. A **594**, 325 (1995).
- [15] E. Oset and A. Ramos, Nucl. Phys. A **635**, 99 (1998).

Table C.8: Pole position of the $I = 0$ $\bar{K}N$ - $\pi\Sigma$ system and the meson-baryon distance in the pole state. $f_\pi = 100, 110$ and 120 MeV cases. Corresponding to Table 3.

Case	(i)	(ii)	(iii)
Kinematics	Non-rela.		Semi-rela.
Potential	NRv1	NRv2	KSW
$f_\pi = 100$			
E_R	1417.3	1418.0	1419.6
$B_{\bar{K}N}$	17.7	17.0	15.4
$\Gamma/2$	23.1	19.8	13.2
$\sqrt{\langle r^2 \rangle}_{\bar{K}N+\pi\Sigma}$	$1.31 - 0.29i$	$1.36 - 0.30i$	$1.21 - 0.49i$
$f_\pi = 110$			
E_R	1416.6	1417.8	1420.0
$B_{\bar{K}N}$	18.4	17.2	15.0
$\Gamma/2$	19.5	16.6	12.8
$\sqrt{\langle r^2 \rangle}_{\bar{K}N+\pi\Sigma}$	$1.36 - 0.34i$	$1.42 - 0.34i$	$1.18 - 0.49i$
$f_\pi = 120$			
E_R	1416.9	1418.3	1418.9
$B_{\bar{K}N}$	18.1	16.7	16.1
$\Gamma/2$	16.7	14.0	11.7
$\sqrt{\langle r^2 \rangle}_{\bar{K}N+\pi\Sigma}$	$1.38 - 0.38i$	$1.44 - 0.38i$	$1.16 - 0.42i$

- [16] Summarized in T. Hyodo and D. Jido, Prog. Part. Nucl. Phys. **67**, 55 (2012).
- [17] D. Jido, J. A. Oller, E. Oset, A. Ramos and U. -G. Meißner, Nucl. Phys. A **725**, 181 (2003).
- [18] T. Hyodo and W. Weise, Phys. Rev. C **77**, 035204 (2008).
- [19] V. K. Magas, E. Oset and A. Ramos, Phys. Rev. Lett. **95**, 052301 (2005).
D. Jido, E. Oset and T. Sekihara, Eur. Phys. J. A **42**, 257 (2009).
T. Hyodo, A. Hosaka, E. Oset, A. Ramos and M. J. Vicente Vacas, Phys. Rev. C **68**, 065203 (2003).
- [20] M. Bazzi *et al.* (SIDDHARTA collaboration), Phys. Lett. B **704**, 113 (2011); Nucl. Phys. A **881**, 88 (2012).
- [21] D. W. Thomas, A. Engler, H. E. Fisk and R. W. Kraemer, Nucl. Phys. B **56**, 15 (1973). R. J. Hemingway, Nucl. Phys. B **253**, 742 (1985). S.

Table C.9: Range parameters for $I = 1$ $\bar{K}N$ - $\pi\Sigma$ - $\pi\Lambda$ system with non-relativistic kinematics (left three columns) and semi-relativistic kinematics (right three columns). $f_\pi = 100$ -120 MeV case. Corresponding to Tables 4 and 5.

Case	(ii)			(iii)		
Kinematics	Non-rela.			Semi-rela.		
Potential	NRv2			KSW		
Condition	(a)	(b)	(c)	(a)	(b)	(c)
$f_\pi = 100$						
$d_{\bar{K}N, \bar{K}N}$	0.501	0.501	0.501	0.421	0.421	0.421
$d_{\pi\Sigma, \pi\Sigma}$	0.186	0.695	0.695	0.277	0.395	0.395
$d_{\bar{K}N, \pi\Lambda}$	0.289	0.394	0.663	0.335	0.174	0.100
Re $a_{\bar{K}N (I=1)}$	0.367	0.368	0.626	0.366	0.057	-0.153
Im $a_{\bar{K}N (I=1)}$	0.601	1.452	0.600	0.601	0.189	0.351
$f_\pi = 110$						
$d_{\bar{K}N, \bar{K}N}$	0.438	0.438	0.438	0.369	0.369	0.369
$d_{\pi\Sigma, \pi\Sigma}$	0.159	0.636	0.636	0.248	0.348	0.348
$d_{\bar{K}N, \pi\Lambda}$	0.221	0.301	0.445	0.276	0.157	0.104
Re $a_{\bar{K}N (I=1)}$	0.376	0.372	0.657	0.369	0.075	-0.134
Im $a_{\bar{K}N (I=1)}$	0.606	1.504	0.599	0.600	0.154	0.337
$f_\pi = 120$						
$d_{\bar{K}N, \bar{K}N}$	0.384	0.384	0.384	0.327	0.327	0.327
$d_{\pi\Sigma, \pi\Sigma}$	0.139	0.581	0.581	0.223	0.310	0.310
$d_{\bar{K}N, \pi\Lambda}$	0.173	0.240	0.324	0.236	0.140	0.105
Re $a_{\bar{K}N (I=1)}$	0.382	0.369	0.689	0.379	0.123	-0.097
Im $a_{\bar{K}N (I=1)}$	0.608	1.539	0.601	0.600	0.141	0.360

Prakhov *et al.* (Crystal Ball collaboration), Phys. Rev. C **70**, 034605 (2004). I. Zychor *et al.*, Phys. Lett. B **660**, 167 (2008).

- [22] Y. Ikeda, T. Hyodo and W. Weise, Phys. Lett. B **706**, 63 (2011); Nucl. Phys. A **881**, 98 (2012).
- [23] S. Aoyama, T. Myo, K. Kato, and K. Ikeda, Prog. Theor. Phys. **116**, 1 (2006).
- [24] T. Myo, R. Ando and K. Kato, Phys. Lett. B **691**, 150 (2010).
- [25] A. T. Kruppa, R. Suzuki and K. Kato, Phys. Rev. C **75**, 044602 (2007).

- [26] A. D. Martin, Nucl. Phys. B **179**, 33 (1981).
- [27] A. Doté, T. Inoue and T. Myo, Proceedings of “International conference on the structure of baryons (BARYONS’10) ”, AIP Conference Proceedings Volume 1388, page 589. (ISBN: 978-0-7354-0952-1)
- [28] R. Suzuki, A. T. Kruppa, B. G. Giraud and K. Kato, Prog. Theor. Phys. **119**, 949 (2008).
- [29] J. Yamagata-Sekihara, J. Nieves and E. Oset, Phys. Rev. D **83**, 014003 (2011).
- [30] T. Sekihara, T. Hyodo and D. Jido, Phys. Rev. C **83**, 055202 (2011).
- [31] S. Takeuchi and K. Shimizu, Phys. Rev. C **79**, 045204 (2009).
- [32] M. Homma, T. Myo and K. Kato, Prog. Theor. Phys. **97**, 561 (1997) and references therein.
- [33] Private communication with Dr. Hyodo.
- [34] Y. Ikeda, T. Hyodo, D. Jido, H. Kamano, T. Sato and K. Yazaki, Prog. Theor. Phys. **125**, 1205 (2011).
- [35] S. Aoyama, Phys. Rev. C **68**, 034313 (2003).
- [36] Y. Ikeda and T. Sato, Phys. Rev. C **79**, 035201 (2009).
- [37] SIDDHARTA-2 collaboration. Ref. [40] in the reference [20].
- [38] M. Bayar, C. W. Xiao, T. Hyodo, A. Doté, M. Oka, E. Oset, arXiv:1205.2275 [hep-ph]